Technical

Final Report
F-B2368

Report

A BASIC STUDY OF COLD WELDING IN ULTRAHIGH VACUUM

by

H. Conrad*
L. Rice**

May 30, 1969

Sponsored by

OFFICE OF NAVAL RESEARCH

Contract No. Nonr 4825 (00), NR 031–078

DISTRIBUTION OF THIS DOCUMENT IS UNLIMITED.

*Presently at the University of Kentucky, Lexington, Kentucky.
**Presently at the Aerospace Corporation, El Segundo, California.

THE FRANKLIN INSTITUTE RESEARCH LABORATORIES
BENJAMIN FRANKLIN PARKWAY • PHILADELPHIA, PENNA. 19103

86

ABSTRACT

The cohesion of the FCC metals Ag, Al, Cu, and Ni under ultrahigh vacuum in the range of 10^{-11} to 10^{-9} torr was investigated using the technique of cold welding specimens previously fractured in the vacuum. The cohesion strength of the weld increased with compression load for all metals; all data fell on one curve of slight positive curvature when the cohesion load (stress) and the compression load (stress) were divided by the initial fracture load (stress) of the virgin specimen. The effect of compression load on the cohesion coefficient α for all metals could be described by

$$\alpha = 0.75 + 0.15\ L_C/L_{F_o}$$

where L_C is the compression load and L_{F_o} is the initial fracture load. Ultrasonic measurements on Cu indicated that the contact area was proportional to the ratio L_C/L_{F_o}. Optical microscopy observations on the weld interface were in accord with this; they also indicated the excellent matching of the two fractured surfaces possible with the present apparatus. The cohesion results are explained on the basis that the rupture of the weld occurs at a constant value of the "true" fracture stress.

Limited studies were conducted with Cu to determine the effects of: (1) a subsequent heat treatment on the weld strength, (2) alloying with 30% Zn and (3) exposure of the freshly fractured surfaces to the gases N_2, O_2, CO, CO_2 and air. The heat treatments reduced the strength of the weld; the 70-30 brass alloy exhibited a lower cohesion coefficient than unalloyed Cu; prolonged exposure to the gases O_2, CO, CO_2 and air caused an appreciable reduction in the cohesion coefficient, whereas no effect was observed for N_2. The adverse effects noted for the first two variables are not clearly understood at this time. The results for the exposure to the gases are in good agreement with predictions based on absorption theory and LEED observations reported in the literature.

TABLE OF CONTENTS

LIST OF FIGURES

LIST OF FIGURES (Cont'd)

LIST OF FIGURES (Cont'd)

LIST OF FIGURES (Cont'd)

LIST OF TABLES

1. INTRODUCTION

From a technological viewpoint, an understanding of the cohesion (or adhesion*) of metals is important to such areas as friction and wear, and bonding, joining and cladding. In addition, the subject of the cohesion of metals in ultrahigh vacuum (defined here as a pressure $<10^{-8}$ torr (1)) has become especially important in recent years because it relates to the behavior of components and systems in a space environment and to the possibility of joining materials in space by cold welding (2). Besides having a direct bearing on technology, studies of the cohesion of metals can also provide information concerning the nature and behavior of surfaces, which is of value to understanding such phenomena as catalysis, oxidation and corrosion. This relationwhip between studies of cohesion (and adhesion) to other surface phenomena and technology is illustrated in Fig. 1.

The objective of the present research program was to develop a better understanding of the cohesion of metals through a study of cold welding under ultrahigh vacuum and to establish the influence of certain gaseous environments on this cohesion. The studies have concentrated on metals and an alloy with the FCC crystal structure, namely Ag, Al, Cu, Ni, and Cu70Zn30 brass. As seen from Table I, these materials represent a range in such properties as electronic structure, elastic modulus, stacking fault energy and surface energy, which could be important in cohesion. Moreover, the materials were tested in conditions and with microstructures representing a range of mechanical properties (Table II), since this variable has been claimed to be of importance in cohesion. Finally, for all of these materials, room temperature is below the temperature where self diffusion is expected to play a significant role.

The effects of gaseous environment and alloying were only investigated for Cu. The gases considered were N_2, O_2, CO, CO_2 and air, and the alloy was cartridge brass (Cu70Zn30). The gases represent a range of adsorption energies and type of adsorption with respect to Cu, Table III.

---

* The term cohesion will be used to refer to the bonding of a metal or alloy to itself, while adhesion will refer to the bonding of dissimilar metals or alloys.

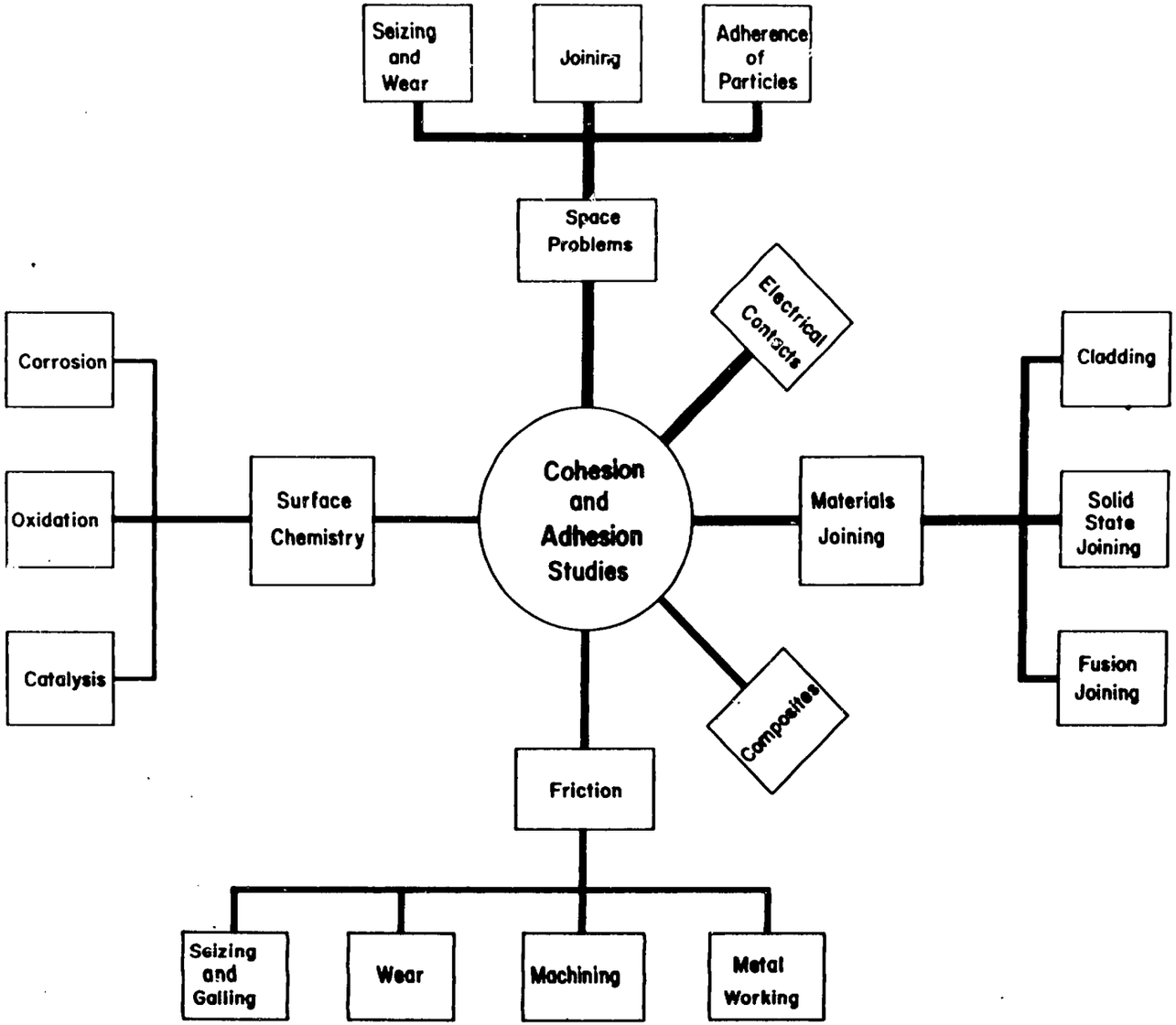

Fig. 1 Technological importance of adhesion and cohesion studies. Relative width of lines is indicative of the degree of direct applicability of the results of present studies to a given technological phenomenon.

TABLE I. SOME PHYSICAL PROPERTIES OF THE FCC METALS WHICH WERE INVESTIGATED

Material	Type	Atomic Number	Outer Electronic Structure	Closest Approach of Atoms[1] A^o	Melting Temperature[1] ^oK	Youngs Modulus[1] $x10^3$ Kg/mm^2	Stacking Fault Energy[2,3] ergs/cm^2	Surface Energy[4] ergs/cm^2
Ag	Noble	47	$4d^{10}5s^1$	2.89	1234	7.8	16-65	1140
Cu	Noble	29	$3d^{10}4s^1$	2.56	1356	11.3	40-120	1670-2892
A1	Group IIIA	13	$3s^23p^1$	3.86	933	6.3	170-238	—
Ni	Transition	28	$3d^84s^2$	2.49	1726	21.1	64-410	1850
Cu70Zn30	Hume-Rothery	—	—	2.60	1188	11.3	5-10	—

References

1. ASM Metals Handbook Vol 1 8th Edition (1961).
2. H. Conrad, *High Strength Materials,* Wiley p. 436 (1965).
3. P. R. Swann, *Electron Microscopy and Strength of Crystals,* Wiley p. 131 (1963).
4. J. M. Blakely and P. S. Maiya, *Surfaces and Interfaces,* Syracuse Press p. 325 (1967).
5. A. Bondi, Chem Rev. *52* 417 (1953).

TABLE II. CONDITION AND MECHANICAL PROPERTIES OF THE FCC MATERIALS USED IN PRESENT INVESTIGATION (1).

Condition	Grain Size μ	Hardness VHN 10 Kg	N_2 (760) torr				Ultrahigh Vacuum (2-10 x 10^{-11} torr			
			Y.S.[2] Ksi	T.S.[3] Ksi	F.S.[4] Ksi	R.A.[5] %	Y.S.[2] Ksi	T.S.[3] Ksi	F.S.[4] Ksi	R.A.[5] %
Commercial Tough Pitch Cu-98%										
AR(C.W.)[6]	–	115	–	79.7	113.9	31	–	79.8	105.2	28
AR + 1 hr. @600°C	9-10	55	15.7	41.7	81.0	59	15.7	41.0	79.1	59
AR + 1 hr. @950°C	50	54	13.1	39.3	79.4	59	11.9	38.6	75.5	58
Commercial OFHC Cu-99,9+%										
AR(C.W.)	–	122	–	87.1	198.3	56	–	87.5	184.1	52
AR + 1 hr. @350°C	6-7	53	20.6	43.5	142.5	82	27.4	46.8	137.4	77
AR + 1 hr. @600°C	100	44	10.9	38.5	124.4	81	15.0	40.9	129.5	79
AS & R High Purity Cu-99,9+%										
AR + Straighten	350	45	23.8	34.3	195.8	92	–	—	—	–
AR + Swage 75%	—	100	—	66.9	318.5	79	–	65.8	272.9	76
AR + 1 hr. @600°C	450	41	11.5	36.9	144.5	92	12.0	39.4	162.5	86

Notes:

(1) Specimen dimensions given in Fig. 2

(2) Load at 10^{-3} in. plastic elongation divided by initial cross section area at root of notch, A_o.

(3) Maximum load divided by A_o.

(4) Load divided by cross section area at root of notch at fracture, A_{F_o}.

(5) Reduction in Area = $\frac{A_o - A_{F_o}}{A_o} \times 100$

(6) AR = As-received: C. W. = Cold worked.

TABLE II. CONDITION AND MECHANICAL PROPERTIES OF THE FCC MATERIALS USED IN PRESENT INVESTIGATION (1). (CONT'D)

Condition	Grain Size μ	Hardness VHN 10 Kg	N_2 (760) torr				Ultrahigh Vacuum (2-10 x 10^{-11} torr			
			Y.S.[2] Ksi	T.S.[3] Ksi	F.S.[4] Ksi	R.A.[5] %	Y.S.[2] Ksi	T.S.[3] Ksi	F.S.[4] Ksi	R.A.[5] %
Commercial Fine Ag - 99,9+%										
AR + 1 hr. @300°C	15	41	25.4	34.8	121.3	83	26.1	35.9	108.8	81
Commercial 1100 Al										
AR + 1 hr. @360°C	50	29	17.6	22.5	79.8	88	16.1	23.5	71.3	85
Commercial INCO 270 Ni - 99,5+%										
AR (Hot Rolled)	45	83	65.0	79.2	332.4	80	65.9	77.9	317.0	80
Commercial Carthride Brass-Cu70Zn30										
AR + 1 hr @400°C	75	87	60.0	68.8	121.6	44	64.5	72.1	125.8	43

Table III. Adsorption of Gases on Copper

Gas	Heat of Adsorption Kcal/mole	Chemiadsorbed	Ref.
Nitorgen	1.34-5.0	No	1
Carbon Dioxide	?	(Yes)?	1
Carbon Monoxide	9.3-20.0	(Yes)?	1,2,3
Oxygen	110	Yes	

References:

(1) D. O. Hayward and B. M. W. Trapnell, *Chemisorption*, Butterworths, London (1964).

(2) R. A. Beebe and E. L. Wilder, J. Am. Chem. Soc. *56* 642 (1934).

(3) A. W. Smith and J. M. Quets, J. Catalysis *4* 163 (1965).

(4) R. M. Dell, F. S. Stone and P. F. Tiley, Trans. Faraday Soc *49* 195 (1953).

The addition of Zn to Cu lowers the stacking fault energy and the Cu70Zn30 alloy represents a solid solution with short range order.

Since in cohesion studies it is desirable to obtain surfaces which are free of contaminating gases or films, it was decided to investigate the cohesion of specimens which has been previously fractured in a vacuum, similar to the experiments of Ham (3). In this way, clean surfaces can be produced with relative ease and the results obtained with such surfaces provide a reference for comparison with those from surfaces previously contaminated and subsequently cleaned by various means.

2. EXPERIMENTAL PROCEDURE

To localize the fracture and to reduce the amount of necking, a notched speciment of the form shown in Fig. 2 was used. This specimen has a notch geometry and notch sharpness ($\rho/r = 5.0$) similar to those used by Ham (3) and represents the optimum for obtaining a relatively flat fracture with the load at fracture being least sensitive to small changes in notch geometry (4). Specimens of the form shown in Fig. 2 were machined from as-received rods, electropolished in standard solutions, and either tested directly, or annealed in a static vacuum of 10^{-6} torr to produce the desired grain size, electropolished again and tested.

The cold welding tests were conducted in the ultrahigh vacuum testing apparatus shown schematically in Fig. 3. This system is capable of producing a vacuum of 2×10^{-11} torr and applying a maximum load in tension or compression of 1000 lbs. with a load sensitivity of 0.01 lb. and an elongation sensitivity of 2×10^{-4} in. To apply both tensile and compressive loads to the specimen and to ensure good mating of the two fracture surfaces during the joining stage, the gripping and alignment fixture shown in Fig. 4 was employed.

Previous to conducting the cohesion studies, the mechanical testing machine was calibrated using a hardened steel rod. This established the elastic behavior of the machine (which was relatively soft) and provided corrections which could be applied to the test data to separate machine effects from the behavior of the specimen. The bellows were arranged so that no corrections were needed to account for their contraction or expansion. Specimen elongations were all measured from the cross-head motion of the testing machine.

The materials employed, their metallurgical condition, hardness and mechanical properties for the notched specimen are listed in Table II. In the case of Cu, a rather wide range of structures, grain sizes and mechanical properties were included. The mechanical properties were for

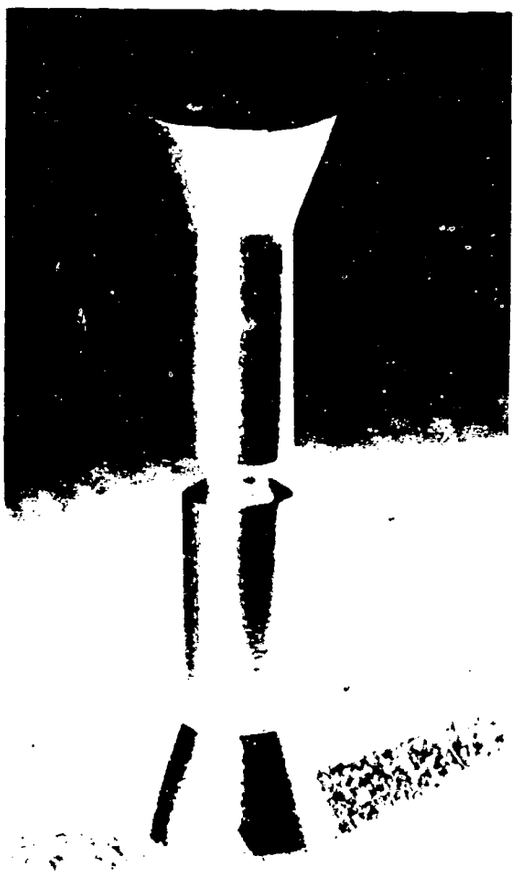

Photograph of actual specimen

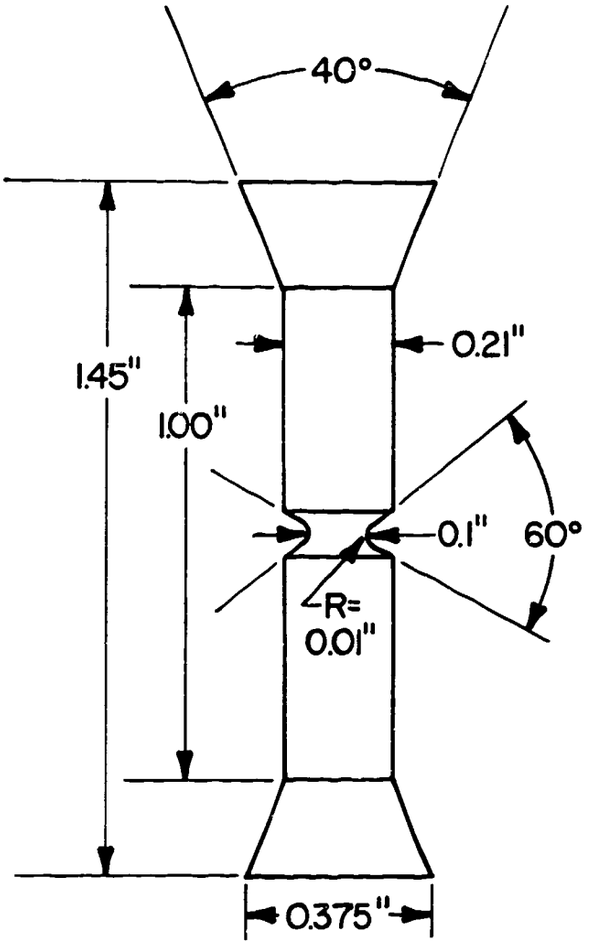

Dimensions of Specimen

Fig. 2 Specimen Employed in Present Tests

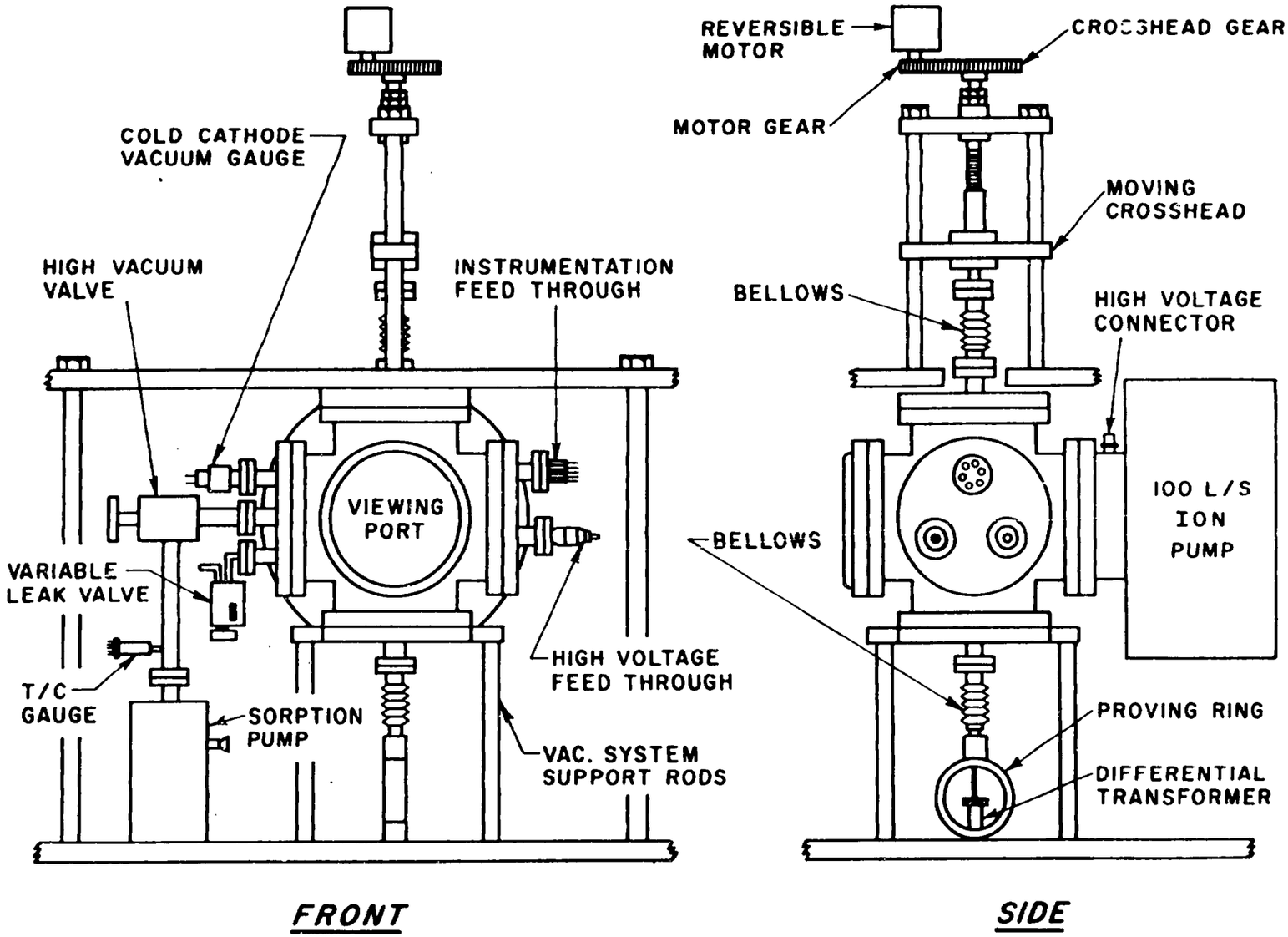

Fig. 3. Schematic of the Ultrahigh Vacuum Test Equipment

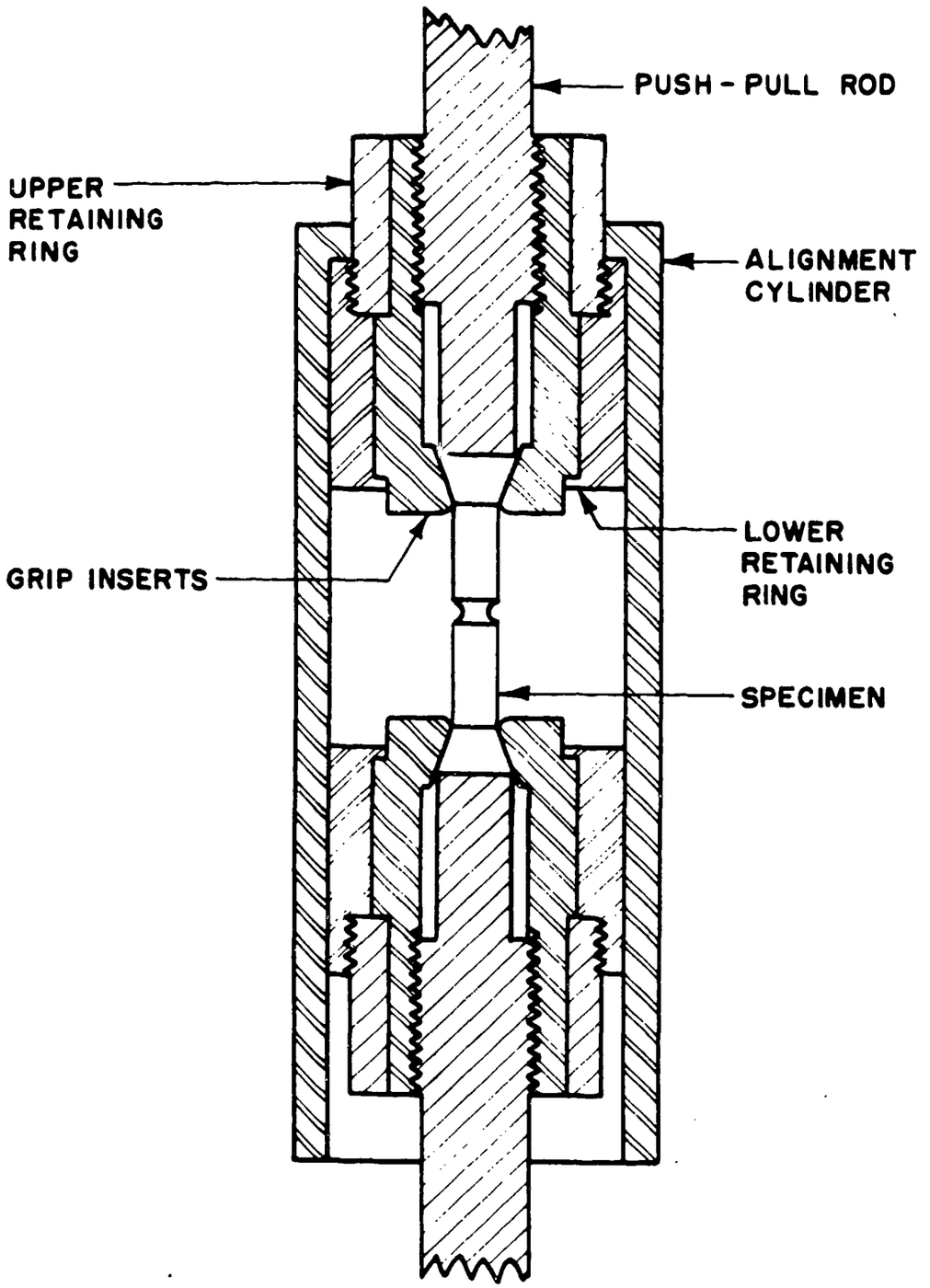

Fig. 4. Schematic of Specimen Grips and Alignment Fixture

the most part reproducible to within 10%, there was essentially no difference between the properties in N_2 at atmospheric pressure and in ultrahigh vacuum. The tensile strength is roughly proportional to the hardness (Fig. 5); however, no such direct correlation exists between yield strength and hardness or fracture strength and hardness. In the case of Cu, where this was checked, the average strength values in air at atmospheric pressure were about 10% higher than those listed in Table II for the N_2 and ultrahigh vacuum environments. This feature is covered in more detail later in the report.

A standard cohesion test consisted of pulling a specimen to fracture at a constant crosshead velocity of 0.01 in. per min. under an ultrahigh vacuum* (after initially flushing the system with purified dry dry nitrogen† and then baking out at 150°C), exposing the fracture surfaces to the vacuum environment for a predetermined time, pushing the two fractured halves together at the same crosshead speed and to a fixed load, holding the specimen at this load for a fixed time‡, and finally pulling the cold welded specimen apart again (at the same crosshead speed) to ascertain the fracture load of the cold welded specimen, i.e., the degree of cohesion. The load and crosshead displacement associated with the entire test were automatically recorded using a Mosely x-y recorder. All tests were conducted at room temperature. The specimens were only welded and fractured once; i.e. no multiple weld-fracture tests were investigated.

In some cases the change in specimen diameter was measured during the cold welding and subsequent tensile testing cycle, concurrent with crosshead displacement determinations. These diameter measurements were made by sighting with a cathatometer through the porthole in the vacuum system onto the reduced section of the notched specimen. These

---

*The vacuums investigated were in the range 2×10^{-11} to 2×10^{-9} torr; however, most tests were conducted in the range of 2×10^{-11} to 10×10^{-11} torr.

†The purified nitrogen contained 0.001 wt. % 0_2 and 0.0012 wt% H_20, maximum.

‡The time of contact was varied from 5 to 900 seconds; however most tests were conducted with a contact time of 300 seconds.

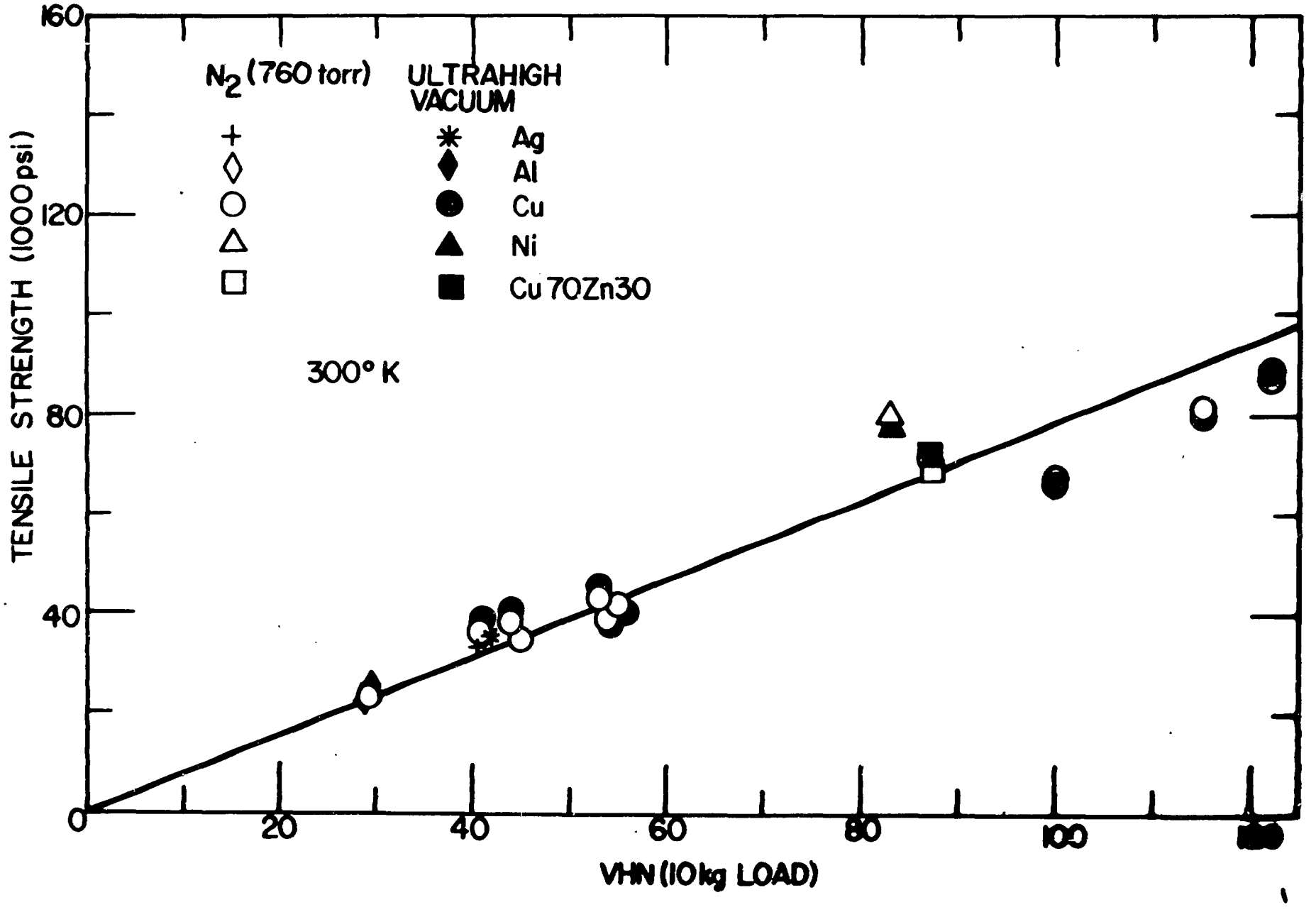

Fig. 5. Tensile Strength Versus Hardness for the FCC Metals Considered

cathatometer readings were accurate to 1×10^{-3} in. An interesting feature of these tests was that the pressure in the chamber increased to about twice its value each time the light was turned on to make a diameter measurement. Upon switching off the light, the pressure decreased again to its previous value.

To establish the contact area nondestructively, some of the copper specimens were removed from the vacuum chamber following cold welding and examined at ambient pressure with a Sperry UM 715 reflectroscope, using the "through transmission technique" with one search unit being applied to each end of the test specimen. In this technique the transmitting search unit projects an ultrasonic beam into the specimen which travels through the material to the opposite surface where it is picked up by the receiving search unit. Any discontinuities in the path of the beam will cause a reduction in the energy (wave amplitude) passing through the specimen to the receiving search unit. Contact between the search crystals and the specimen ends was established using a thin film of glycerine. Some of the specimens were mounted in a metallographic cold mount prior to testing to prevent any damage to the weld, others were tested without such mounting. There was good agreement between the two procedures.

The procedure generally employed for studying the effect of exposure of the fractured surfaces to various gases (N_2, O_2, CO, CO_2 and air) consisted of first obtaining a vacuum of about 2×10^{-11} torr using the usual procedure and then backfilling the chamber with the desired gas to a predetermined pressure. This pressure was then maintained relatively constant during the exposure by manually controlling the addition of the gas through a needle valve keeping the vac-ion pump operating. The exposure times during such tests were generally kept constant between 300 and 600 seconds, requiring pressures between 10^{-10} to 10^{-4} torr to yield the exposures from 10^{-8} to 10^{-2} torr-seconds which were investigated. An exposure of 10^{-1} torr-second for CO was obtained with a time of 2400 seconds at 5×10^{-5} torr. Exposures of 10^{5} torr - second for N_2 and air were obtained by maintaining the gas in the chamber

at atmospheric pressure. A variation of the above procedure consisted of shutting off the pump and the gas inlet valve once the desired pressure had been reached, giving a static system. The cohesion results for this latter procedure were the same as those for the more usual procedure described above. The N_2, O_2, CO and CO_2 gases employed in these studies were of reagent grade.

A limited microscopic study was made of the nature and structure of the weld interface. For this study, Cu specimens were cold welded under the ultrahigh vacuum and then removed from the chamber, after which they were sectioned and prepared for metallographic examination using standard procedures.

3. EXPERIMENTAL RESULTS

3.1 Load Versus Deformation Behavior

Examples of the load versus crosshead travel curves which were observed for the test under ultrahigh vacuum are given in Figs. 6 to 9. Fig. 6 is typical of specimens which were in a cold worked state prior to testing, while Figs. 7 and 8 are representative of the annealed unalloyed specimens. The relatively flat region of the curves near zero load is due to machine effects. The significance of the loads L_{F_o} (load at fracture of the virgin specimen) L_C (maximum compressive load during cold welding) and L_{F_1} (load at fracture of the weld) is indicated. Fig. 9 illustrates the behavior of the 70-30 brass alloy. There were two major differences between the behavior of the brass as compared to the unalloyed metals: (a) serrations indicative of a Portevin-LeChatelier effect occurred during the initial loading to fracture and (b) at fracture the pressure in the vacuum chamber increased an order of magnitude, indicating the release of Zn vapor or some gas. The larger exposure to the environment listed in Fig. 9 as compared to Figs. 6-8 reflects this higher pressure.

An example of the load-deformation behavior during a cold welding and subsequent tensile testing cycle is depicted in Fig. 10, which is a combined plot of the cross-head displacement corrected for machine effects $\Delta \ell_s$, and the change in specimen cross sectional area ΔA, versus the load ratio L/L_{F_o}, where L is the applied load and L_{F_o} is the initial fracture load. To be noted is that only little change in cross sectional area and displacement occurs for compressive loads less than about one-half of the initial fracture load (i.e. for $L_C/L_{F_o} < 0.5$). As the compressive load is increased above $L_C/L_{F_o} > 0.5$, there results a significant increase in both cross sectional area and crosshead displacement. This rapid increase continues to the end of the compressive loading, which generally was taken to $L_C/L_{F_o} \geq 1.10$. During the subsequent unloading, both the area and the displacement decrease in an approximately linear fashion with decrease in load, passing through zero load with an area and displacement somewhat

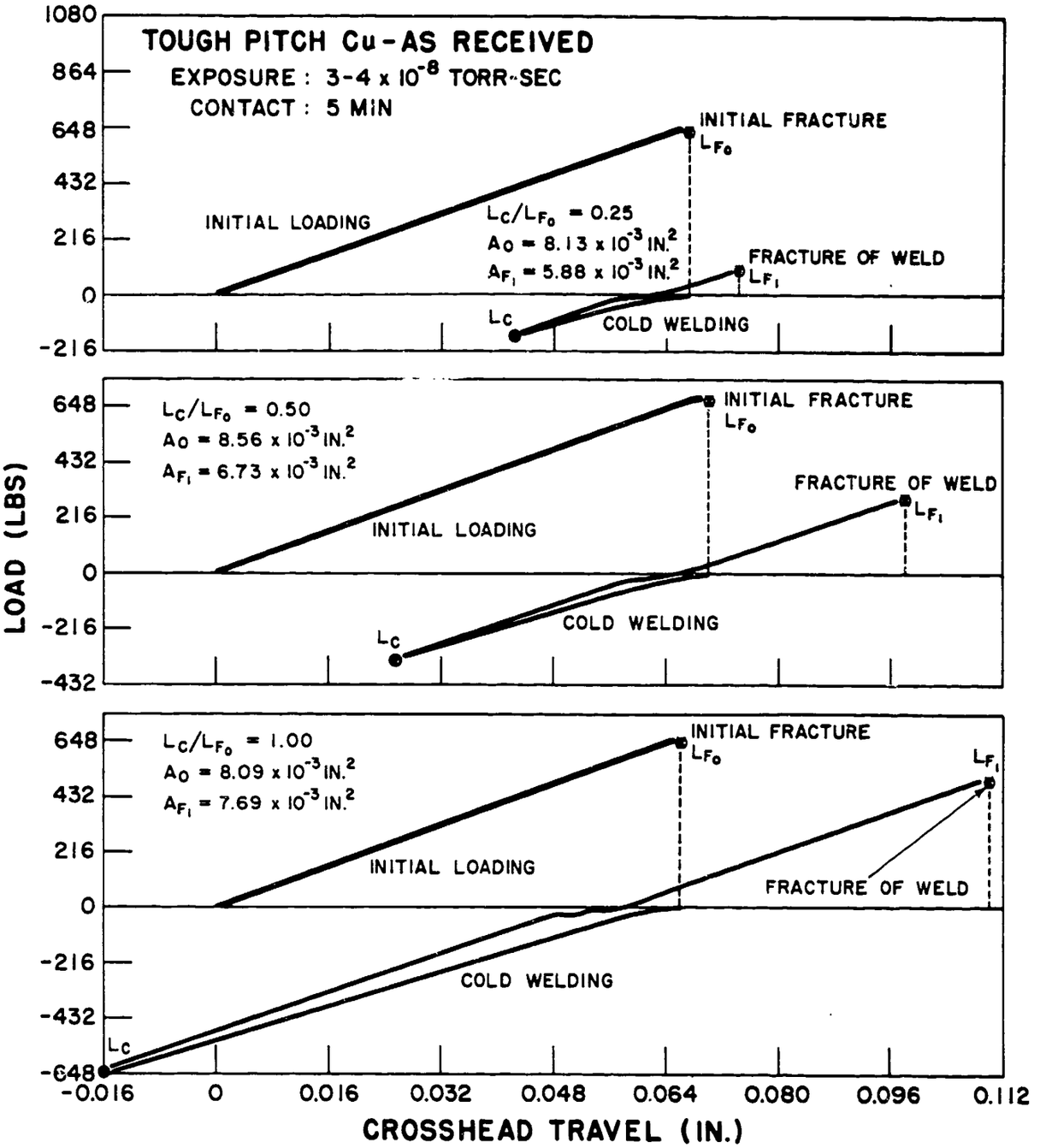

Fig. 6. Load-Crosshead Travel Curves for Initial Fracture, Cold Welding and Subsequent Fracture of the Weld for Cold Worked (As Received) Tough Pitch Copper

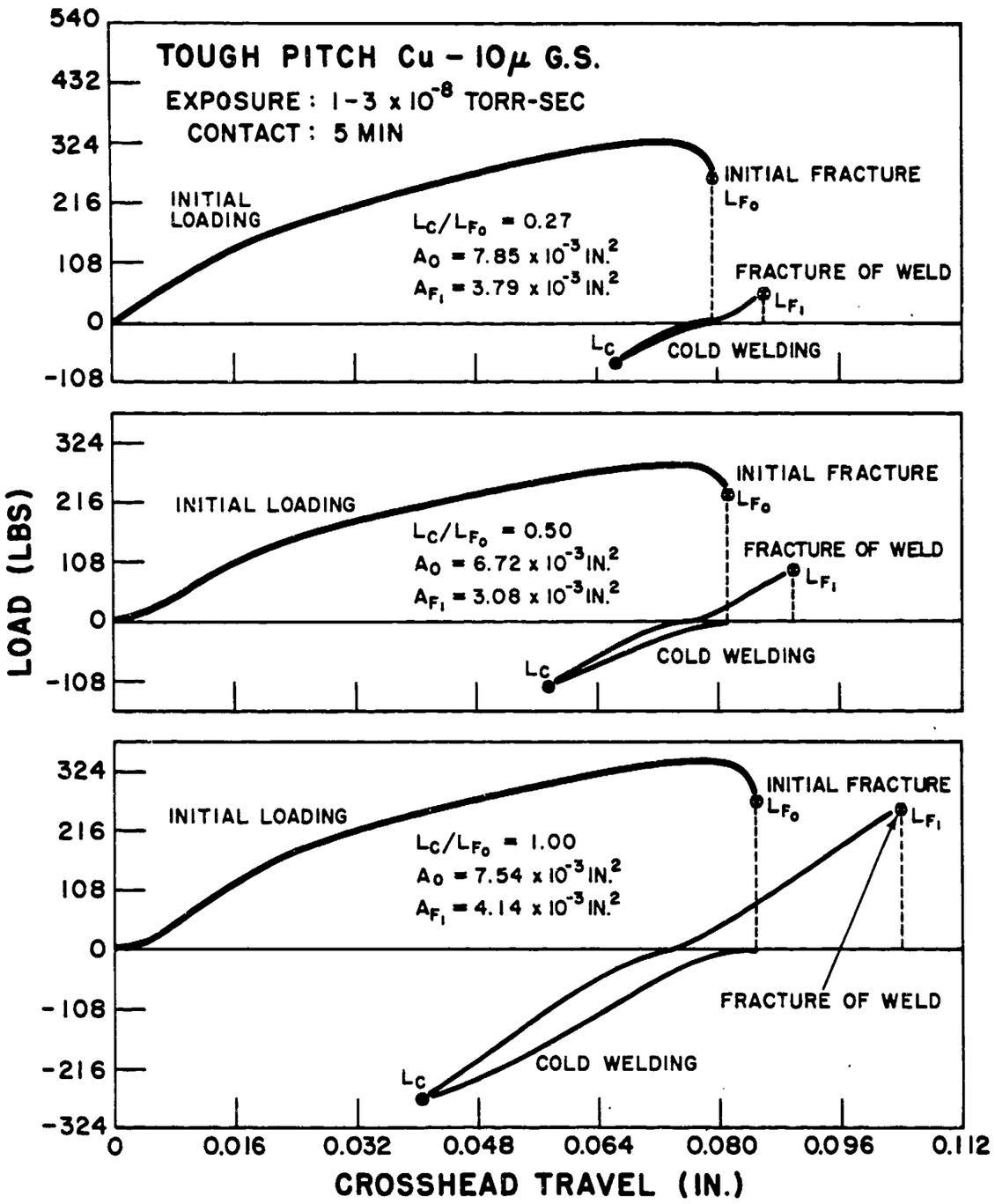

Fig. 7. Load-Crosshead Travel Curves for Initial Fracture, Cold Welding and Subsequent Fracture for Tough Pitch Cu - 10μ G.S.

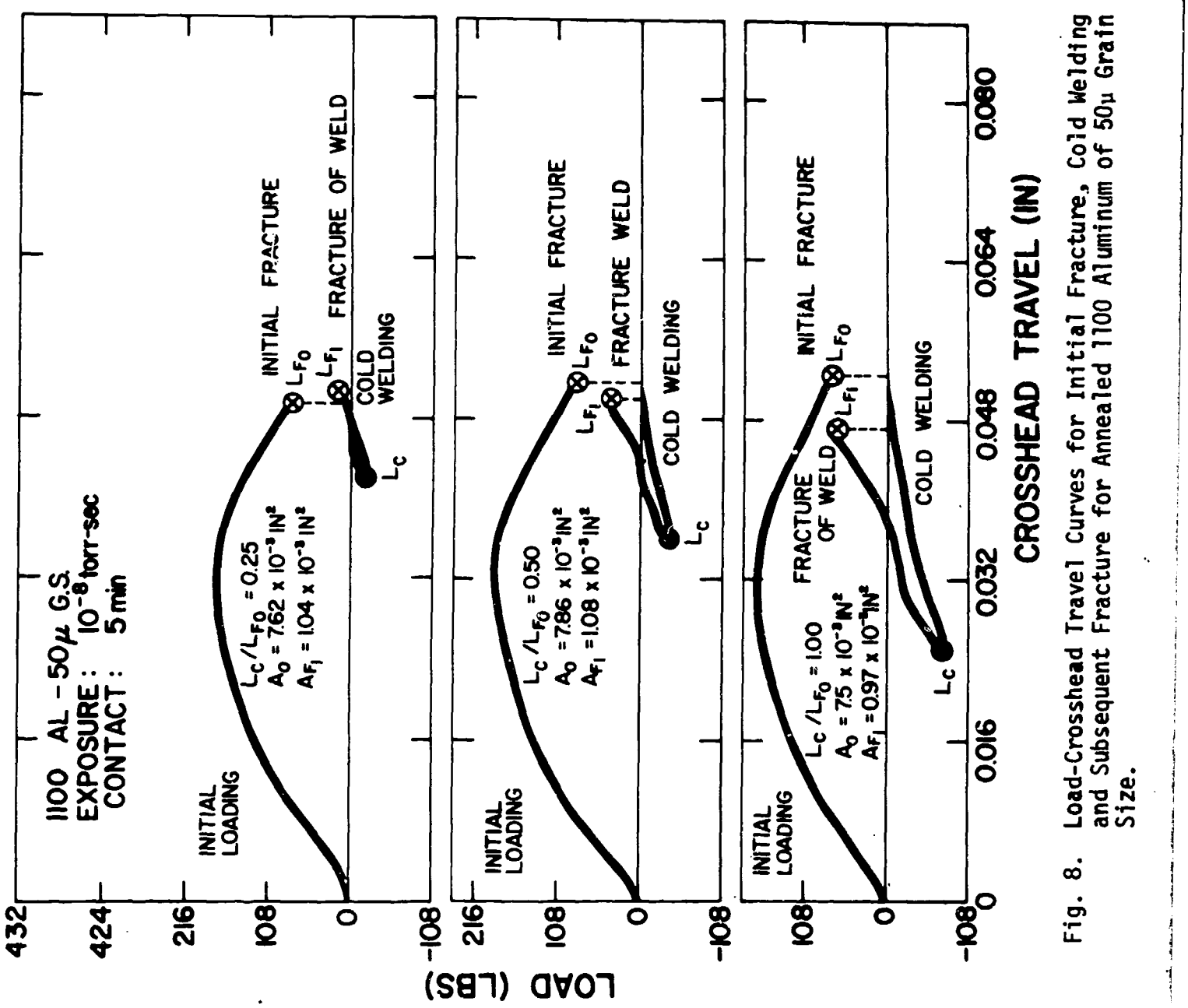

Fig. 8. Load-Crosshead Travel Curves for Initial Fracture, Cold Welding and Subsequent Fracture for Annealed 1100 Aluminum of 50μ Grain Size.

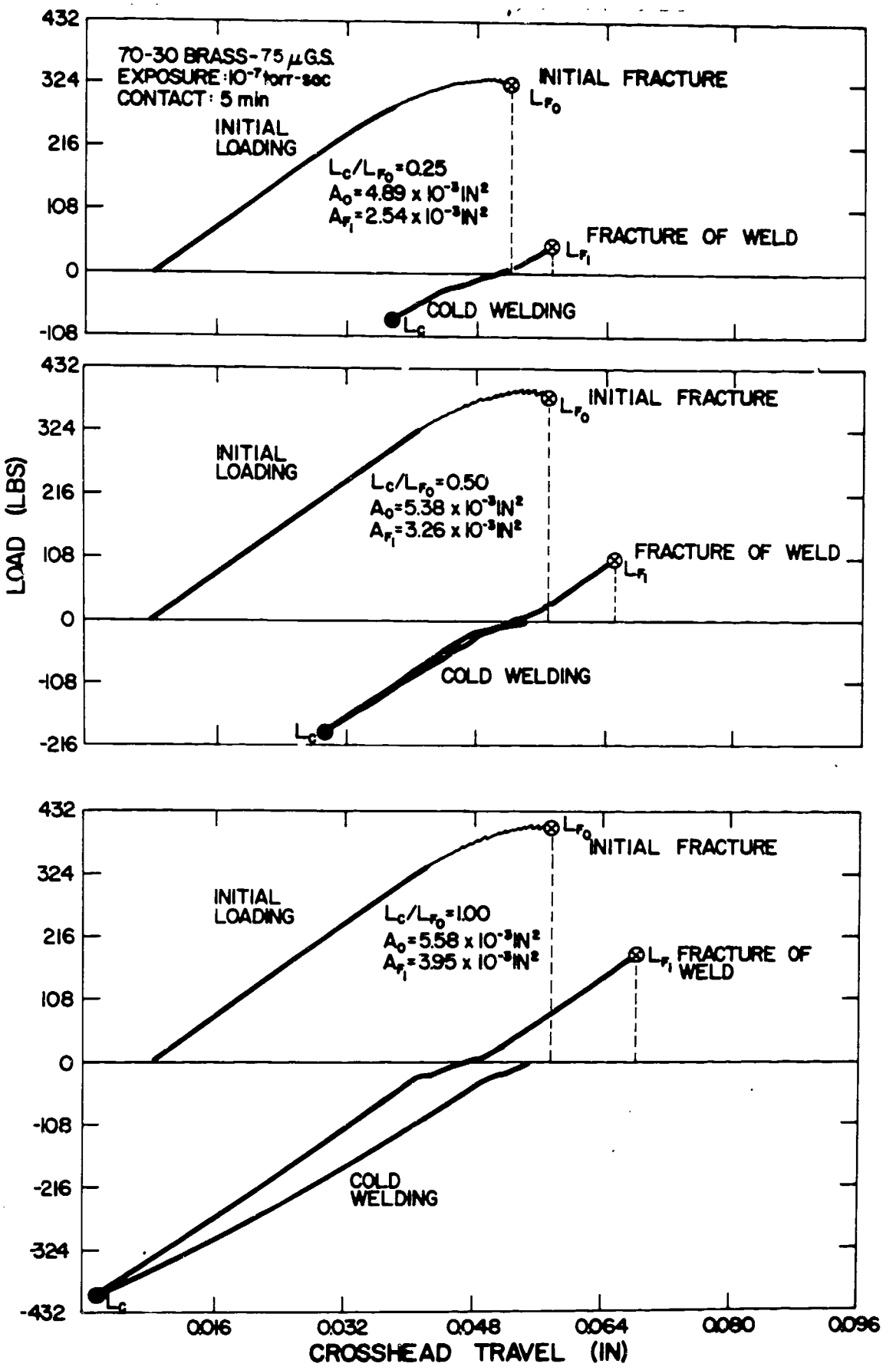

Fig. 9. Load-Crosshead Travel Curves for Initial Fracture, Cold Welding and Subsequent Fracture of the Weld for Annealed 70-30 Brass of 75μ Grain Size.

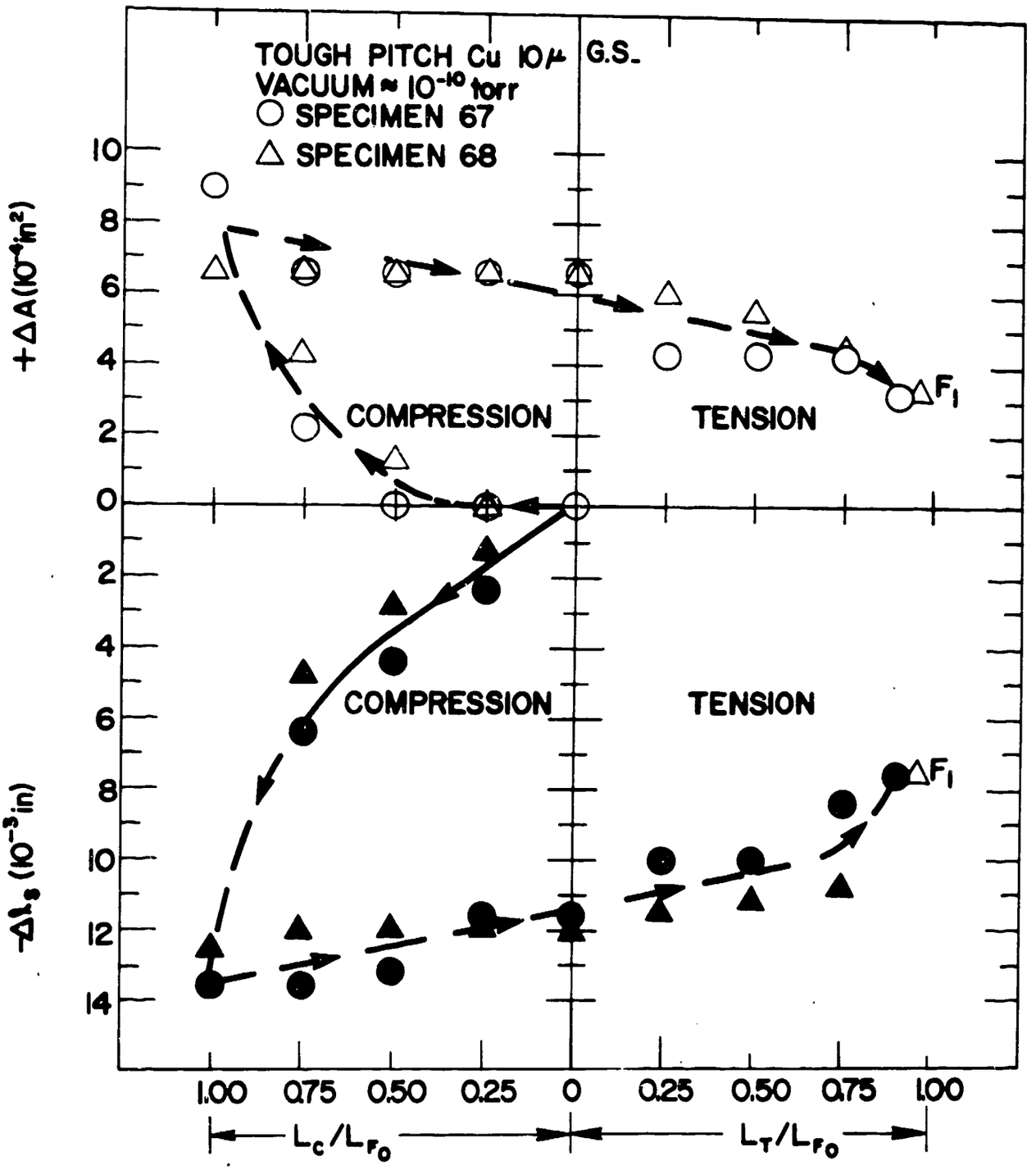

Fig. 10. Corrected Crosshead Displacement $\Delta\ell_s$ and Change in area ΔA at the Root of the Notch as a Function of Load for a Cohesion Test on Annealed Tough Pitfh Copper.

greater than the initial condition. The linear region continues to a tensile load of about 0.5 L_{F_o}. Upon further increase in tensile load, there occurs a more rapid decrease in area and increase in displacement, both of which are approaching the original dimension or position, but do not quite attain them.

The change in cross sectional area ΔA versus the corrected cross-head displacement $\Delta \ell_s$ is depicted in Fig. 11. A log-log plot of these data indicates that ΔA is roughly proportional to $(\Delta \ell_s)^2$ i.e.

$$\Delta A \cong 4.6 \times 10^{-1} \, (\Delta \ell_s)^2$$

Considering ΔA_c to represent the plastic flow which occurs during the compression, it is seen from Fig. 12 that this plastic flow can be considered to be proportional to $(L_C/L_{F_o})^2$ in accord with the stress-strain behavior of many metals (5-7).

The "average" true stress taken as L/A_c during a cohesion test (where A_c was measured by the cathetometer) versus the ratio L/L_{F_o} is plotted in Fig. 13 for four tough pitch copper specimens. Spec. 66 was only compressed to $L_C/L_{F_o} = 0.25$ and Spec. 65 to $L_C/L_{F_o} = 0.5$ prior to tensile testing, whereas the other two specimens were compressed to $L_C/L_{F_o} = 1.0$. To be noted is that all data points lie on a single -curve in the tensile as well as the compressive regions, even though the fracture stress of the weld increases with the ratio L_C/L_{F_o}. Also of significance is that an extrapolation of the tensile portion of the curve to $L_T/L_{F_o} = 1.0$ gives a cohesion stress which is in reasonable accord with the initial fracture strength of the material. Finally, it should be noted that for loads greater than $L/L_{F_o} = 0.5$ the "average" true stress for compression $\bar{\sigma}_C$ is lower than that in tension $\bar{\sigma}_T$. This is due to the fact that during compression there occurs an increase in the area, whereas the opposite occurs during tension. At $L/L_{F_o} = 1.0$ the compression stress $\bar{\sigma}_{C_m}$ is about $0.90 \, \bar{\sigma}_{T_m}$.

3.2 Cohesion Results

One way of comparing the cohesion data on the various materials which only involves measurements of loads and therefore does not include any errors which may be associated with area determinations is to plot the

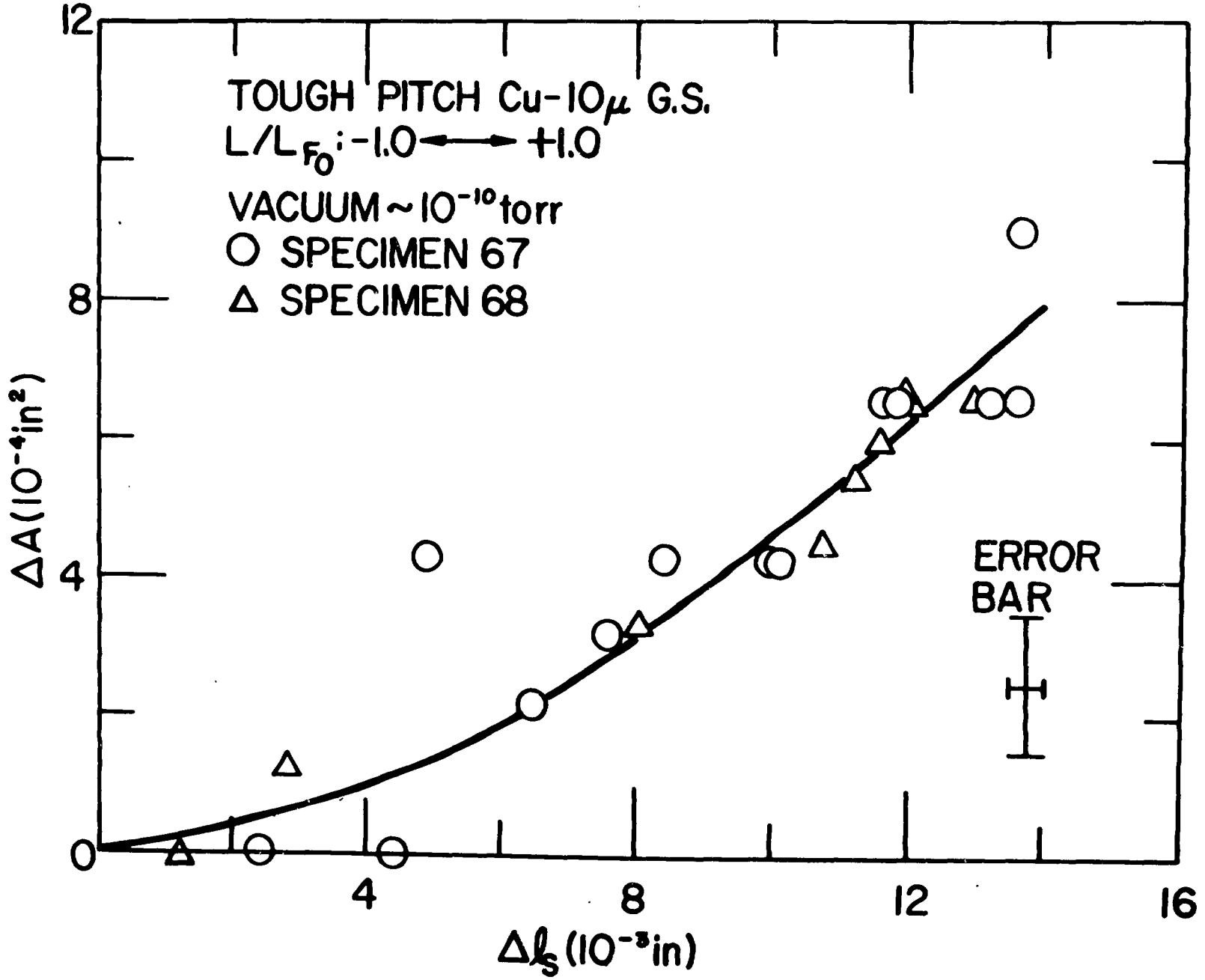

Fig. 11. ΔA Versus $\Delta \ell_S$ for a Cohesion Test on Annealed Tough Pitch Copper

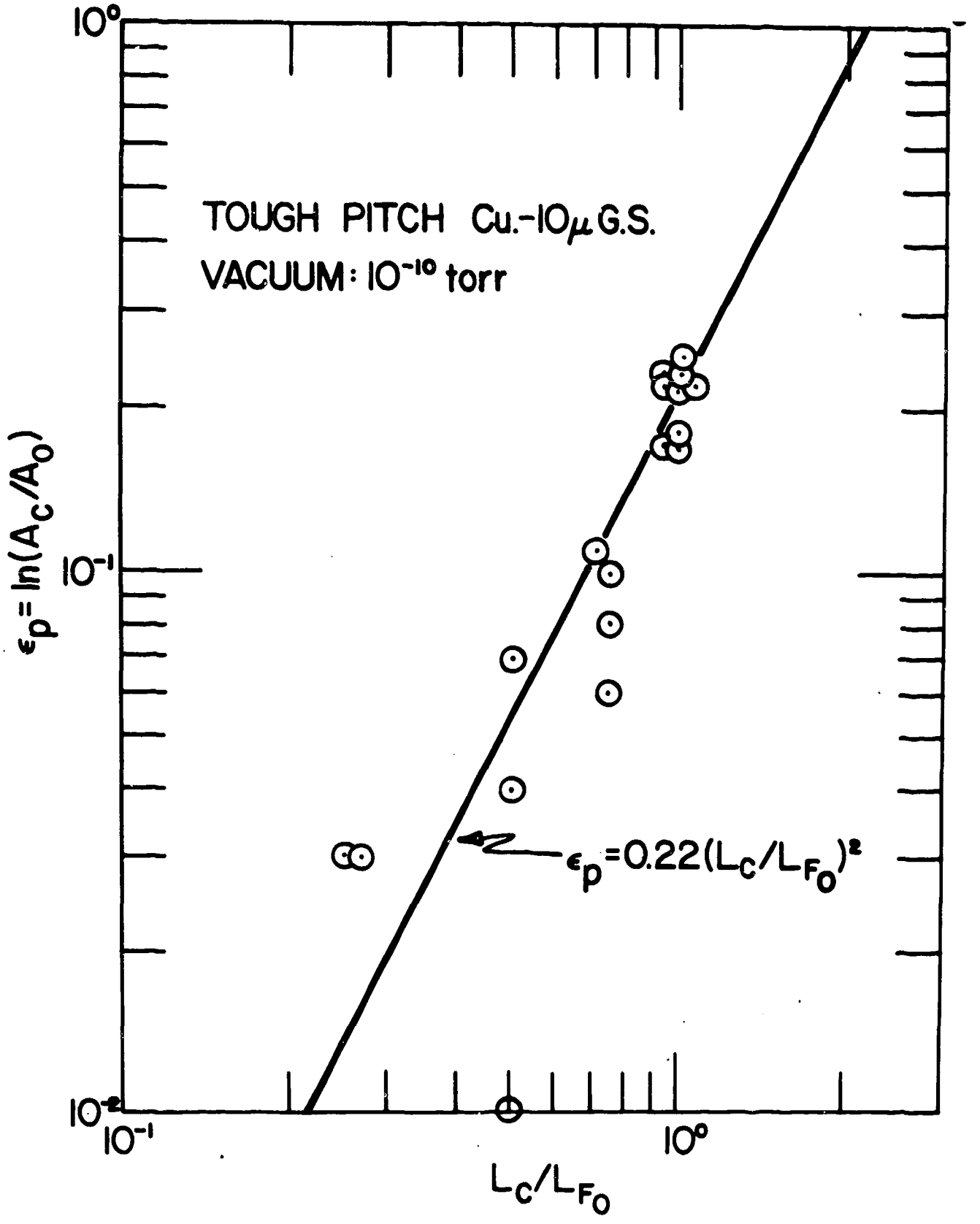

Fig. 12. Plastic Flow During Compressive Loading Versus the Compression Ratio L_c/L_{F_o}

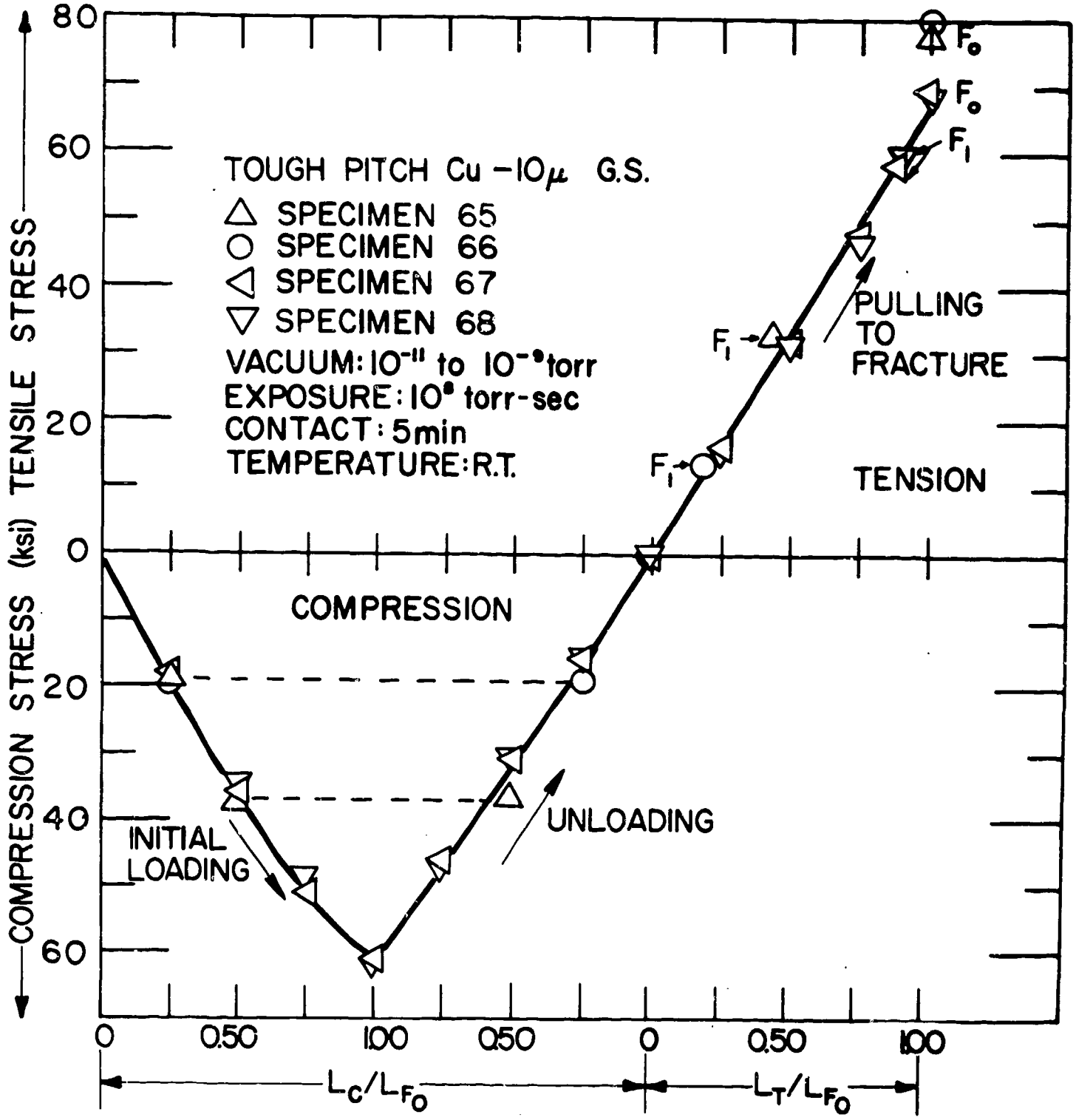

Fig. 13. The Relationship Between "Average" Stress and Load During a Cohesion Test on Annealed Tough Pitch Copper

cohesion ratio $R_F (= L_{F_1}/L_{F_o})$ versus the *compression ratio* $R_C (= L_C/L_{F_o})$. A plot of R_F versus R_C for the tough pitch copper specimens is presented in Fig. 14; a similar plot for all the coppers tested is given in Fig. 15 and for all materials in Fig. 16. Evident from these figures is that for the alloyed FCC metals the cohesion ratio increases with the compression ratio, relatively independent of the purity and struture* of a given metal, and the data for all metals lie on one curve. Also, the curves are not exactly linear, but exhibit a slight positive curvature, especially near the origin. The R_F vs R_C curve for the cartridge brass falls below that for the unalloyed metals; moreover it is more nearly linear (or may even have a slight negative curvature).

The positive curvature in the R_F versus R_C curves for the unalloyed metals is further revealed in Figs. 17 and 18 where the *cohesion coefficient* $\alpha (= L_{F_1}/L_C)$ is plotted versus the compression ration R_C. Within the experimental scatter, α for the unalloyed FCC metals can be considered to increase linearly with R_C yielding.

$$\alpha = 0.75 + 0.15\ R_C \qquad (1)$$

Equally good straight lines were obtained for semi-log and log-log plots of α versus L_C/L_{F_o}. The semilog plot yielded $\alpha = 0.75\ (0.10\ L_C/L_{F_o})$ while the log-log plot gave $\alpha = 0.95\ (L_C/L_{F_o})^{0.18}$. The cohesion coefficient for the Cu70Zn30 brass is less than that for the unalloyed metals and is either independent of the compression ratio or decreases with increase in R_C. There are insufficient data to be certain which is actually the case.

An alternate method of comparing the cohesion results is given in Figs. 19-21, where the "average" cohesion stress $\bar{\sigma}_{F_1}$ $(= L_{F_1}/A_{F_1})$ is plotted versus the "average" compression stress $\bar{\sigma}_C$ $(= L_C/A_{F_1})$. A_{F_1} is the area after fracture of the cold welded specimen. Again, there occurs a slight positive curvature for small compressive stresses in the curve for the

---

*There is a tendency for the cold worked specimens and annealed specimens with grain size greater than 100μ to exhibit lower cohesion ratios.

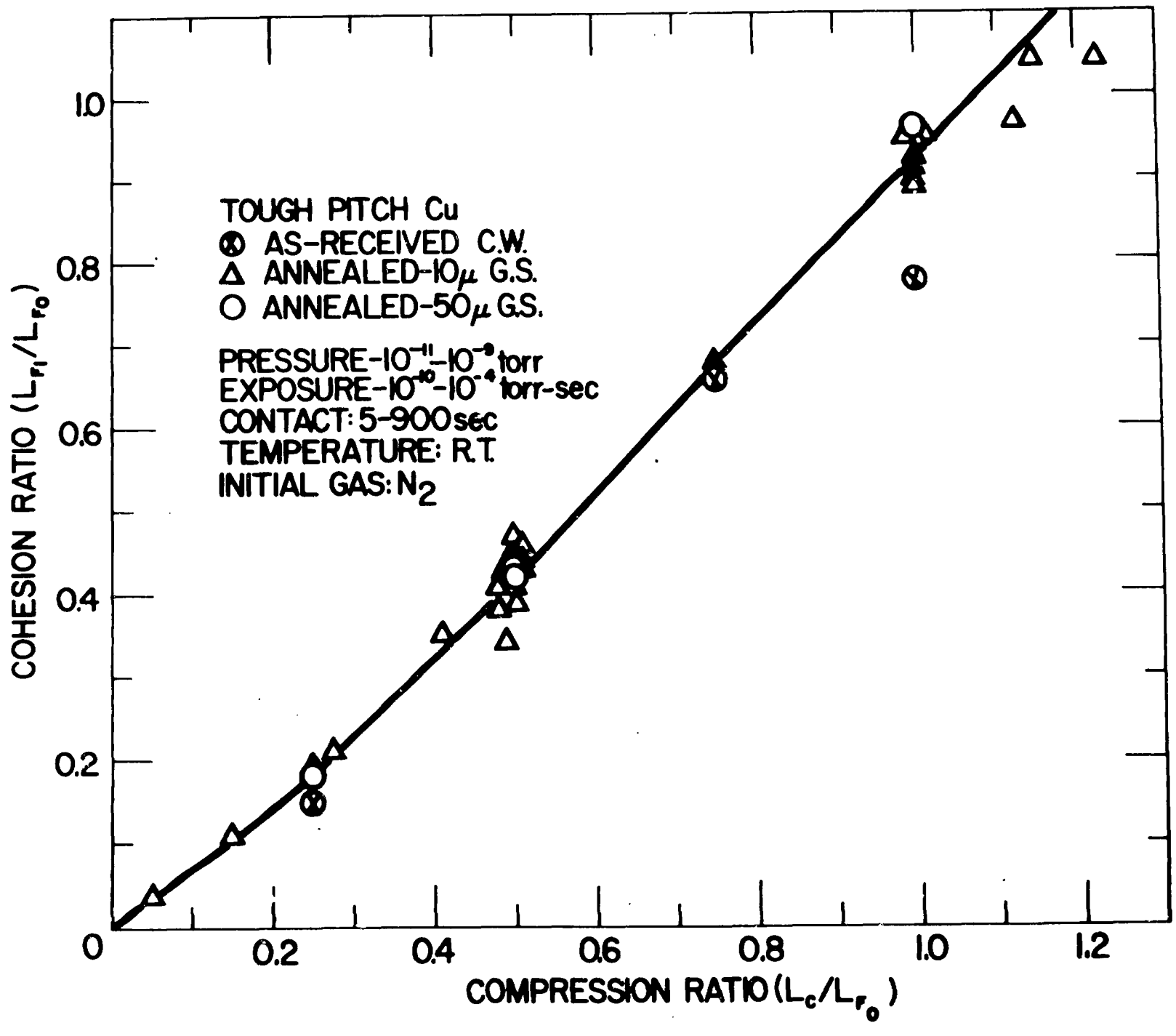

Fig. 14. Cohesion Ratio Versus Compression Ratio For Tough Pitch Copper

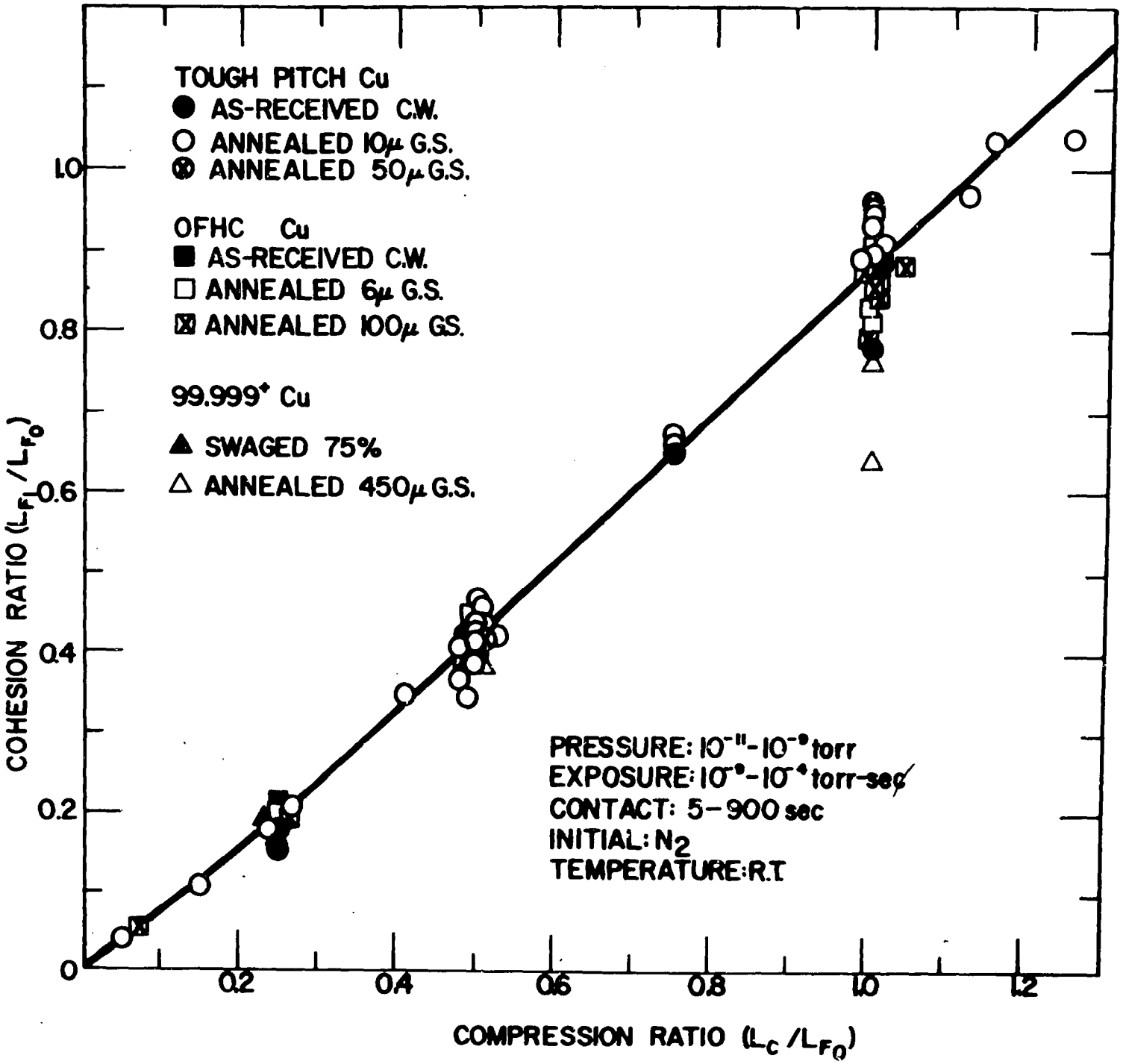

Fig. 15. Cohesion Ratio Versus Compression Ratio For Various Coppers

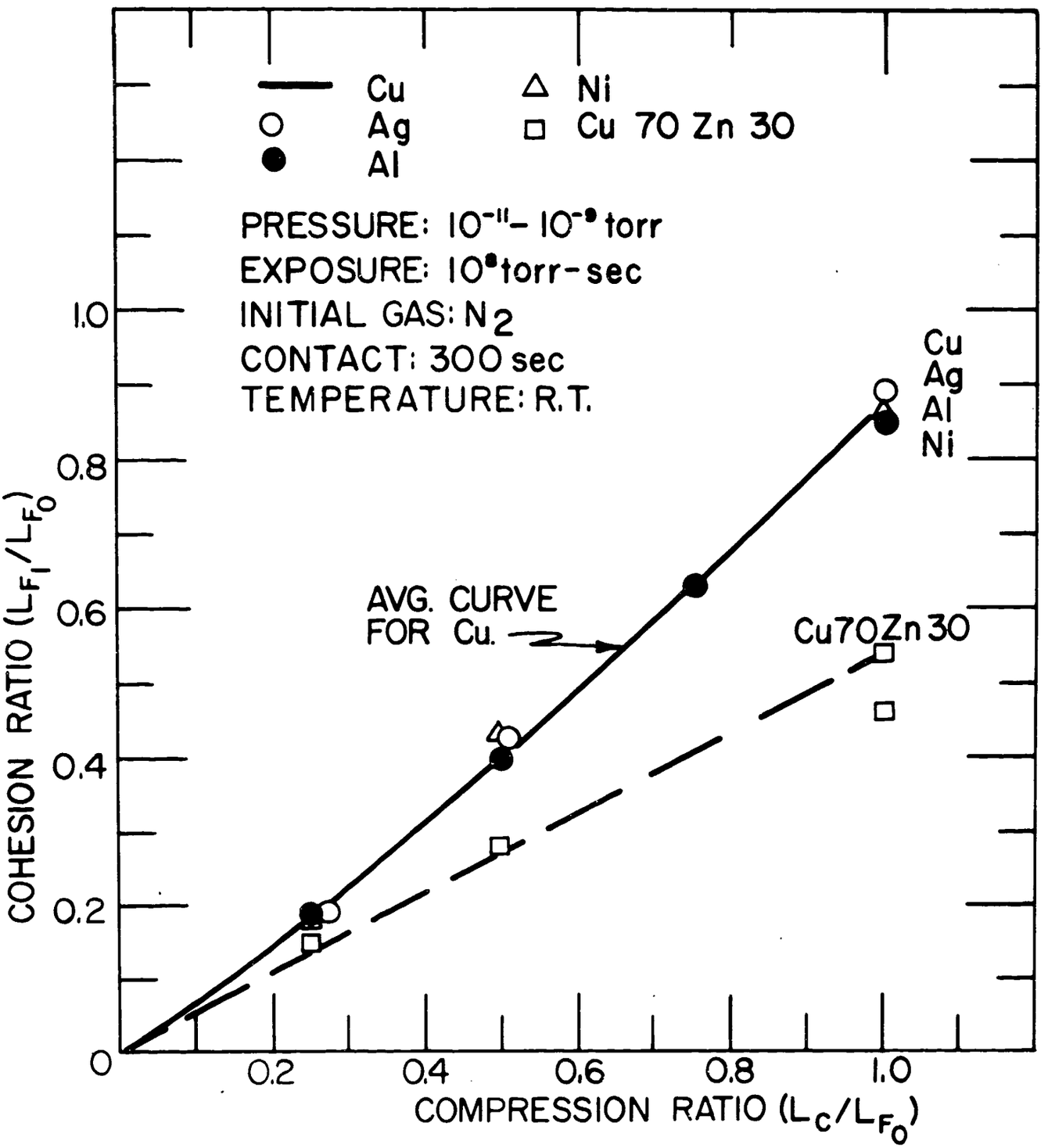

Fig. 16. Cohesion Ratio Versus Compression Ratio For Various FCC Metals and 70-30 Brass

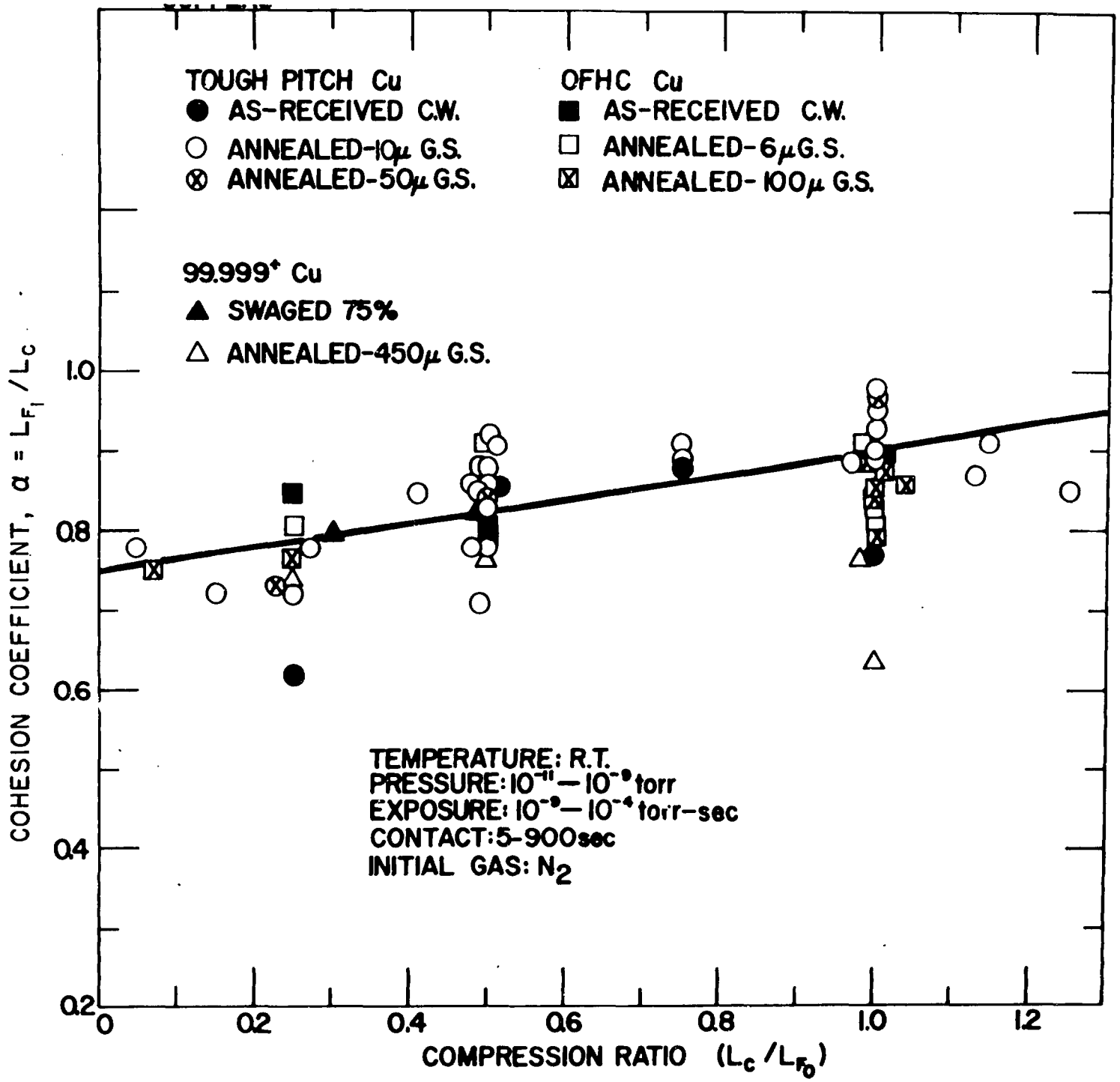

Fig. 17. Effect of Compression Ratio on the Cohesion Coefficient for Various Coppers

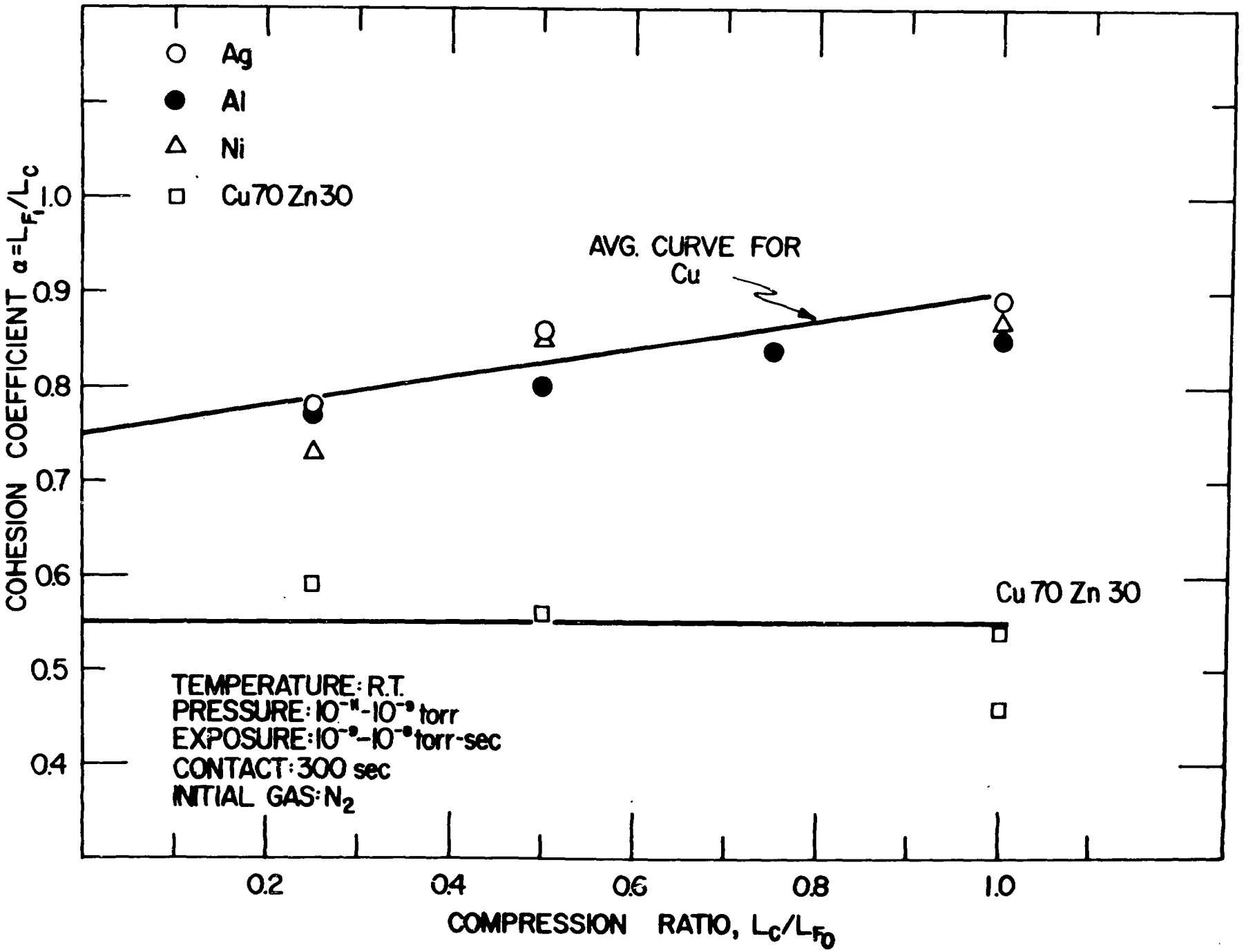

Fig. 18. Effect of Compression Ratio on the Cohesion Coefficient for a Number of FCC Metals and 70-30 Brass

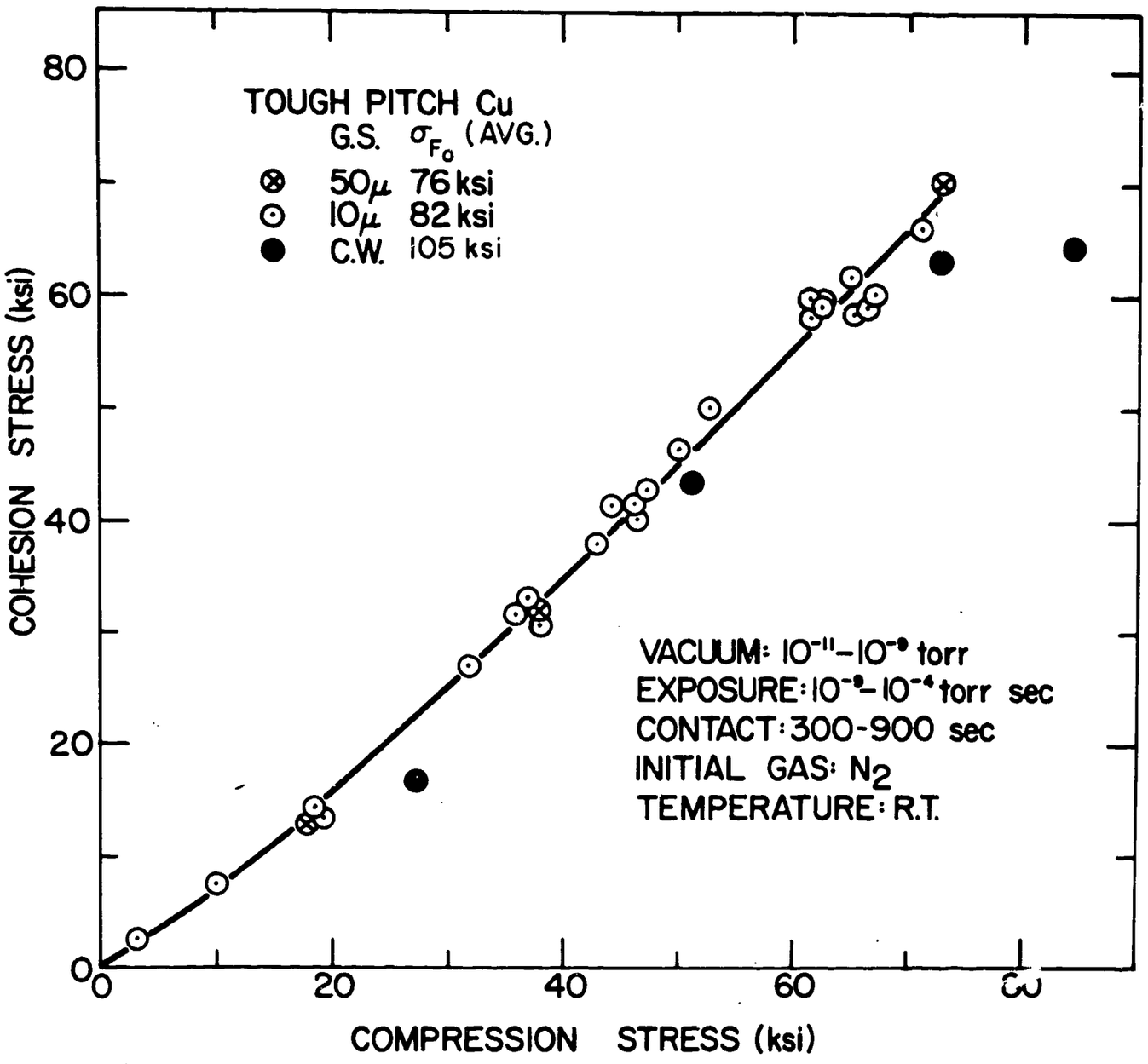

Fig. 19. Effect of Compression Stress on the Cohesion Stress of Tough Pitch Copper

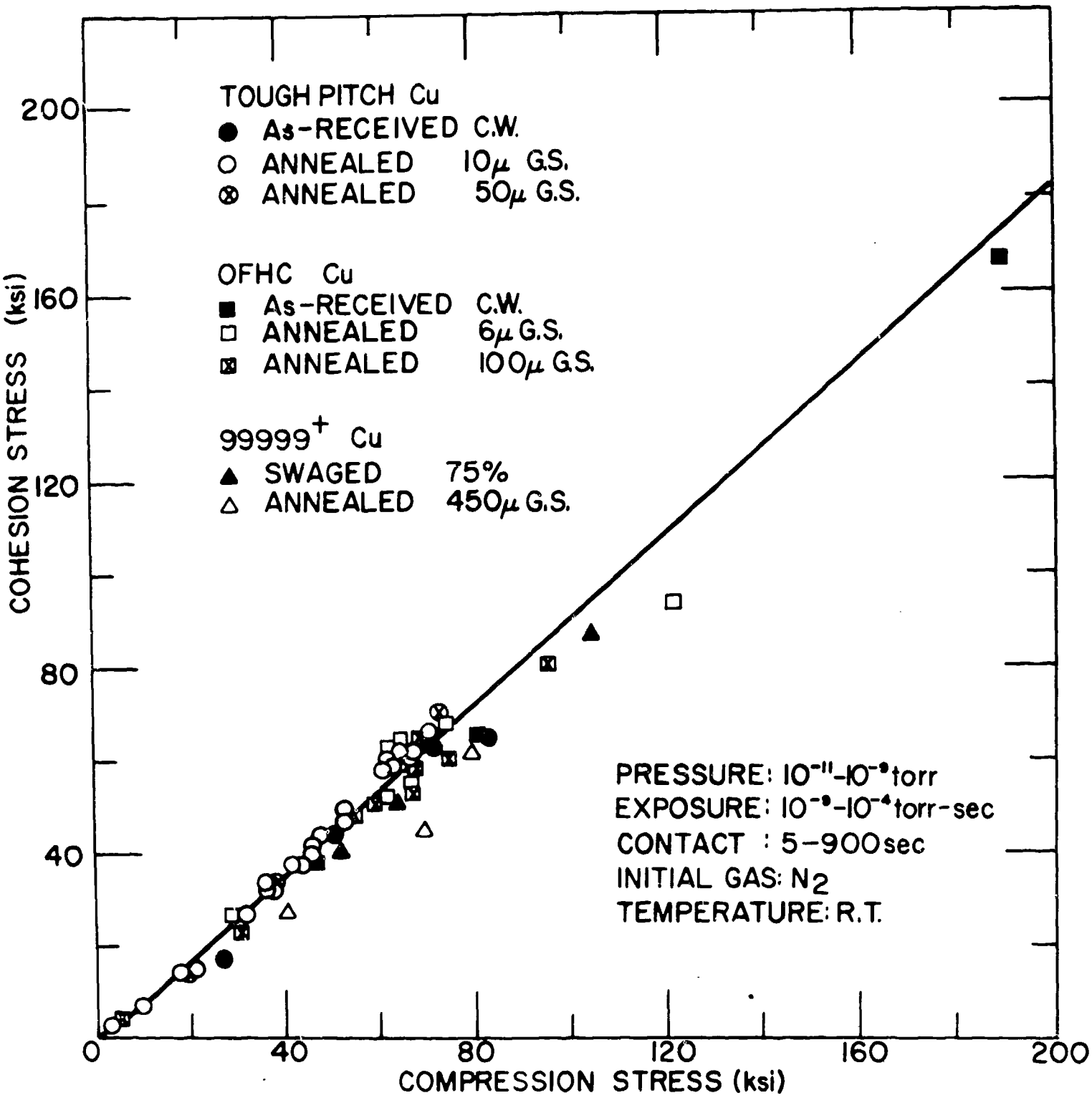

Fig. 20. Cohesion Stress Versus Compression Stress for Various Coppers

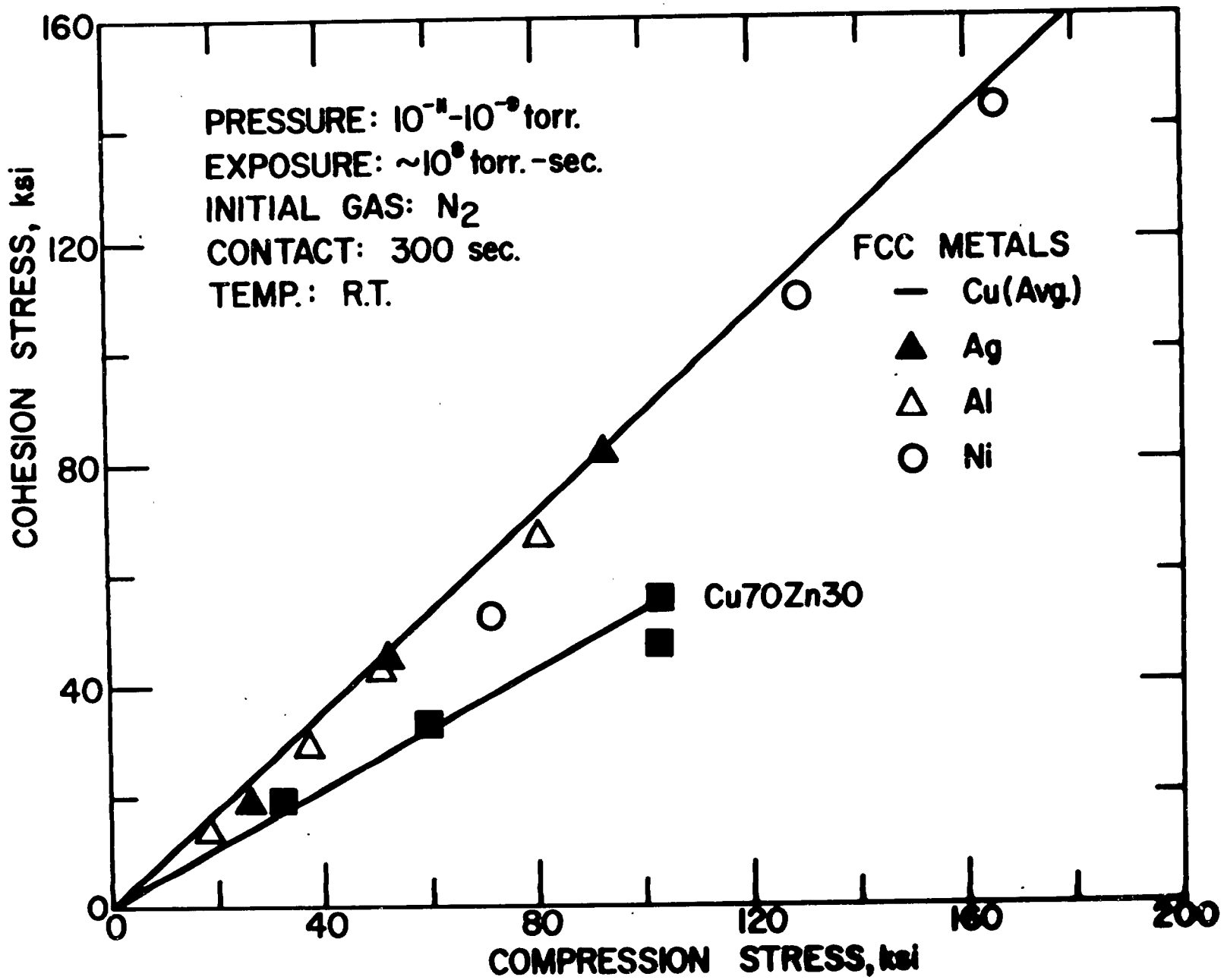

Fig. 21. Cohesion Stress Versus Compression Stress for Several FCC Metals and 70-30 Brass

unalloyed metals, whereas the curve for the brass is either linear or exhibits a negative curvature.

Since the stresses in Figs. 19-21 are based on the final fracture area of the weld, the cohesion coefficient α given by $\bar{\sigma}_{F_1}/\bar{\sigma}_C$ is the same as that defined above by L_{F_1}/L_C. Considering the variation of α with stress, it is found that α increases with the compressive stress, $\bar{\sigma}_C$, from 0.75 at $\bar{\sigma}_C \cong 0$, to 0.90 at $\bar{\sigma} \cong 80{,}000$ psi and then remains essentially constant at this value up to the maximum stress inveatigated of 200,000 psi. Similar results are obtained if the area for the stress determination is taken as the initial fracture area of the virgin specimen A_{F_o}, rather than the final fracture area of the weld A_{F_1}.

Since the diameter of the specimen increases during the compression cycle, the "true" stresses based on the instantaneous area during the compression cycle will be lower than the stress based on either A_{F_o} or A_{F_1}. Consequently, the value of the "true" cohesion coefficient $\alpha_t (=\bar{\sigma}_{F_1}/\bar{\sigma}_{C_t})$ will be larger than that derived only on loads or on stresses based on A_{F_o} or A_{F_1}. This is illustrated in Fig. 22 which gives for the unalloyed metals.

$$\alpha_t = 0.75 + 0.25\ R_C \qquad (2)$$

Of significance is that the value of α_t is approximately 1.0 for $L_C/L_{F_o} = 1.0$. The difference between α and α_t for the Cu70Zn30 is not as large as for the unalloyed metals. Again, α_t may be considered to be independent of R_C or decrease with increase in R_C for the 70-30 Brass.

A very limited study was made of the effect of time of contact (5 to 900 seconds) during the joining of annealed tough pitch copper specimens at $L_C/L_{F_o} = 0.5$. The cohesion coefficient tended to increase with the time of contact. A log-log plot of the cohesion coefficient versus time in seconds yielded

$$\alpha = At^m \qquad (3)$$

with $A = 0.63$ and $m = 0.03$.

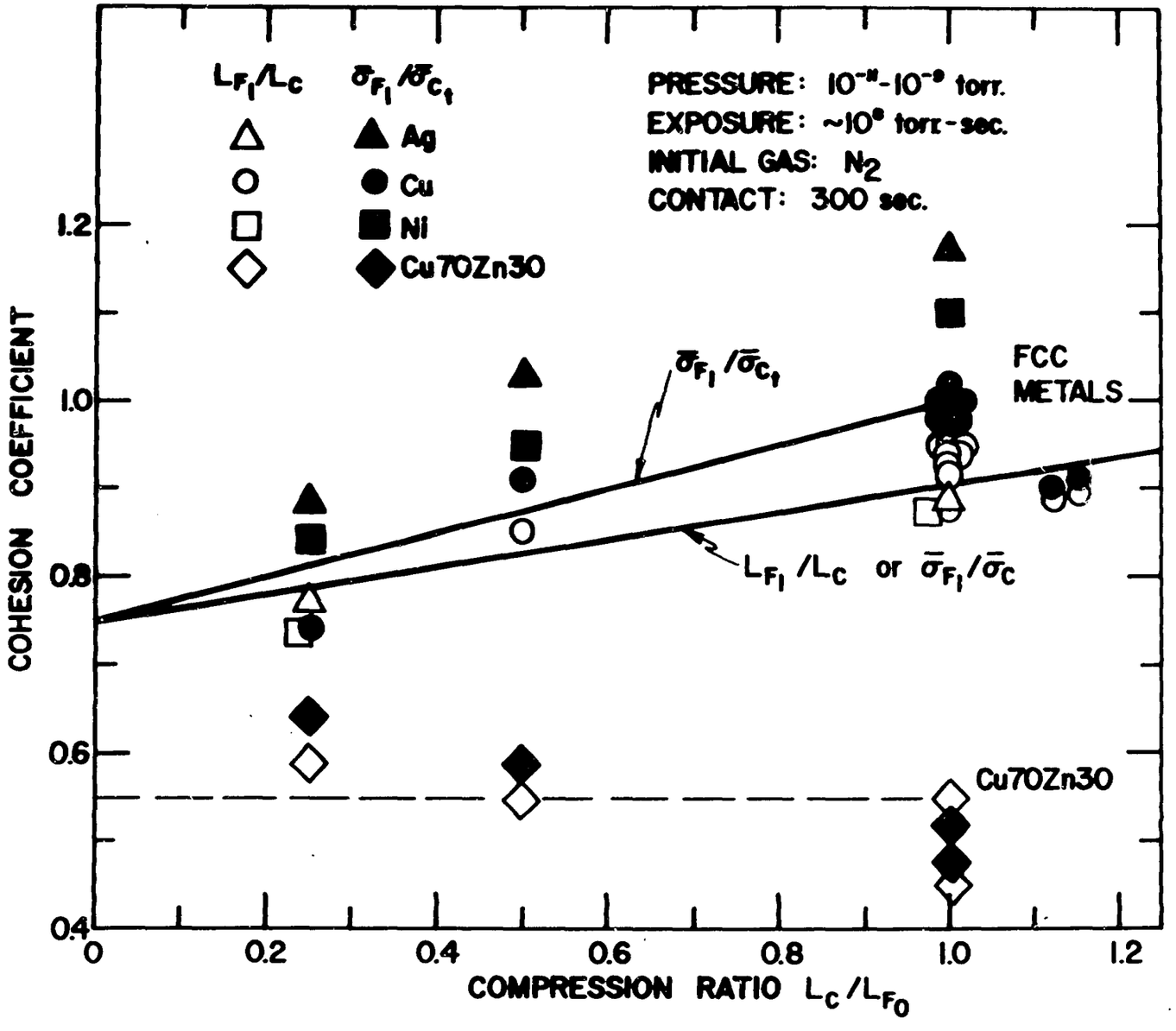

Fig. 22. Cohesion Coefficient Determined by Three Methods Versus the Compression Ratio

3.3 Effect of Environment

The effect of exposing the fractured surfaces of copper specimens to the standard vacuum environment (where the initial gas was high purity nitrogen) is depicted in Fig. 23. Here α_o derived through Eq. 1 is plotted versus the exposure given by the product of the pressure and the time of exposure of thefractured surfaces to the environment. To provide a frame of reference, for a sticking coefficient of 1.0, a monolayer of gas would form after an exposure of about 2×10^{-6} torr-seconds. The pressure and time ranges covered to yield the exposure range in Fig. 23 were 2×10^{-11} to 2×10^{-9} torr and 37 seconds to 6×10^{5} seconds. Evident from this figure is that the cohesion coefficient for copper is independent of the exposure to the vacuum environment.

The effect on the cohesion coefficient α of exposing the freshly fractured surfaces of copper to various gases (N_2, O_2, CO, CO_2 and air) is presented in Fig. 24. For these tests, L_C/L_{F_o} was 1.0 and the joining contact time was 300 seconds. To be noted in Fig. 24 is that exposure to N_2 produces no effect for exposures up to 4.5×10^{5} torr-second at a pressure of 760 torr. For O_2, α begins to decrease after an exposure of about 10^{-5} torr-second and reaches a low value of 0.08 after about 10^{-3} torr-second. The value of α for exposure to air at atmospheric pressure is 0.06, in good agreement with the low value for O_2. For CO and CO_2, a decrease in α first occurs after an exposure of about 10^{-4} torr-second and a minimum of $\alpha = 0.32$ is reached at about 10^{-2} torr-second. The decrease in α from its initial value to its minimum occurs over an exposure range of about two orders of magnitude for the three gases O_2, CO and CO_2.

The studies on the effect of exposure to gaseous environments on cohesion also provided data on the effect of the environment on the mechanical properties of the virgin specimen, for the cohesion specimen was initially pulled to fracture under the environment. The effects of the various gases on the yield stress, tensile strength and fracture stress of a specific batch of annealed tough pitch copper are presented in Fig. 25.

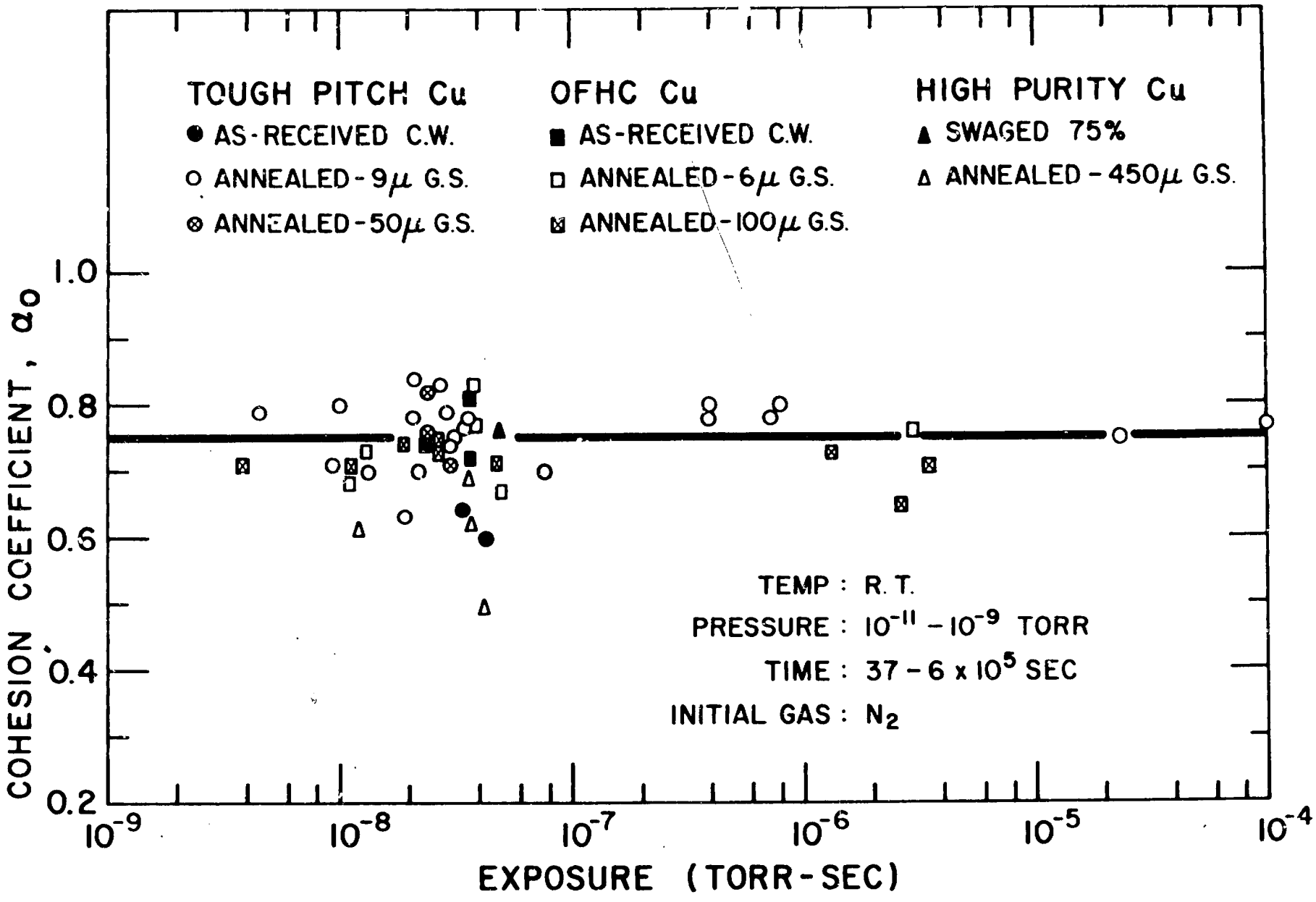

Fig. 23. Effect of Exposure to the Vacuum Environment on the Cohesion Coefficient α_o for Various Coppers

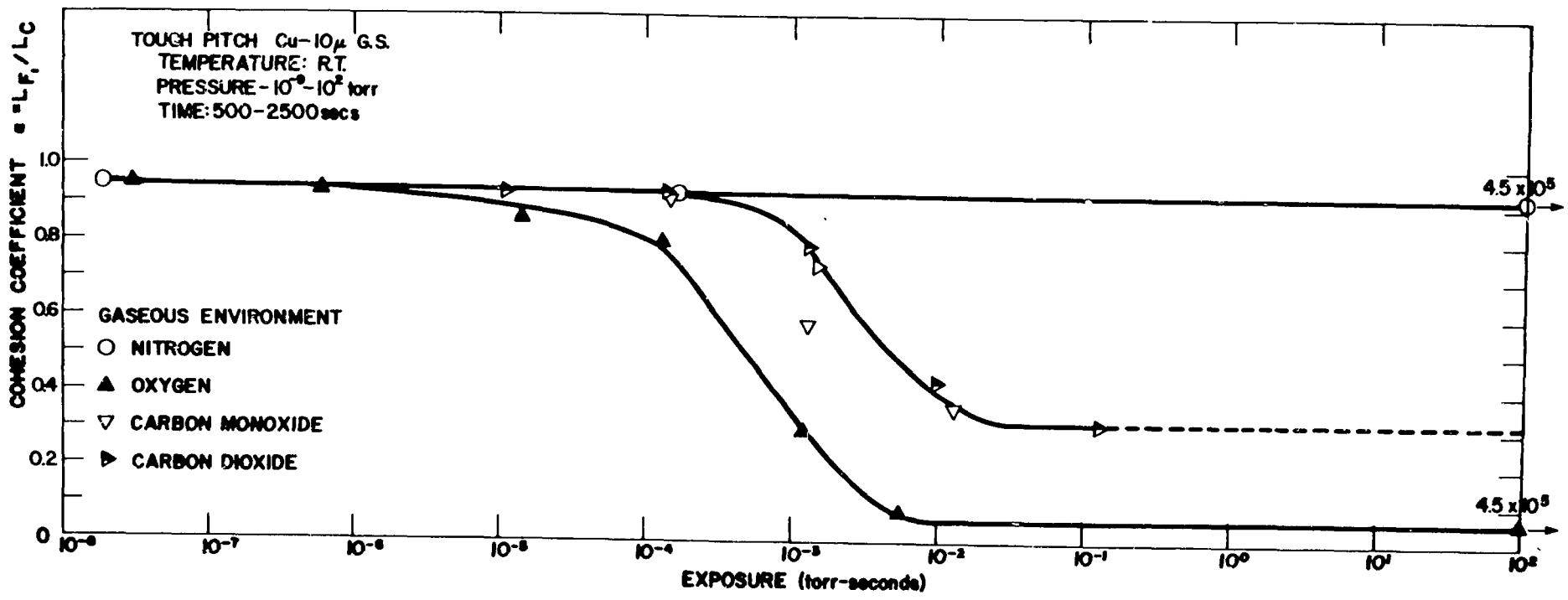

Fig. 24. Effect of Exposure to Various Gases on the Cohesion Coefficient of Annealed Tough Pitch Copper

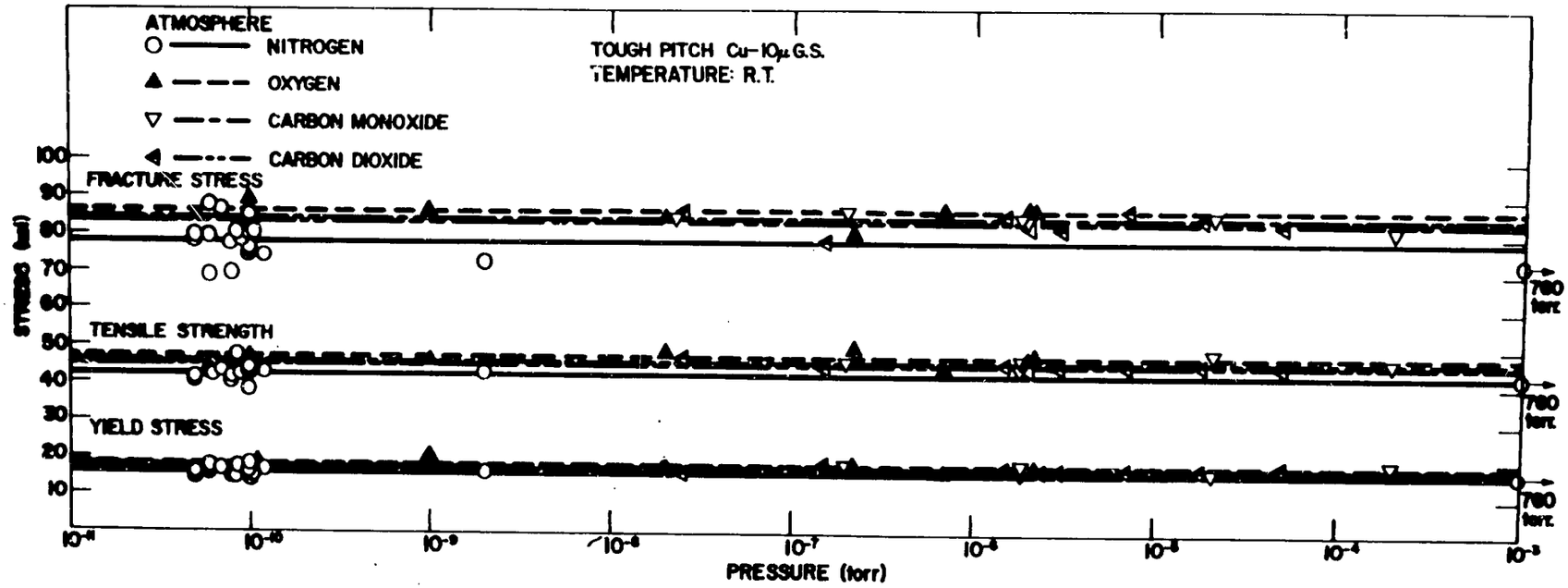

Fig. 25. Effect of Gaseous Environment on the Yield Stress, Tensile Strength and Fracture Stress of Annealed Tough Pitch Copper

To be noted is that the average value for each of these strength parameters is about 10% lower for the N_2 (and for the ultrahigh vacuum) as compared to the other gases over the entire pressure range.

3.4 Ultrasonic Measurements

The results of the ultrasonic measurements are summarized in Figs. 26 to 29. In Fig. 26 it is seen that the ratio of the amplitude of ultrasonic wave for a cold welded specimen λ to that for a virgin specimen pulled to the maximum load (but not fractured) λ_o is approximately proportional to the compression ratio L_C/L_{F_o}. An even better fit to a straight line is obtained if the ultrasonic amplitude ratio is plotted versus the "average" compression stress; see Fig. 27. Of significance here is that the stress at which λ/λ_o becomes equal to 1.0 is within the scatter of the values of the fracture stress for this batch of specimens.

Fig. 28 is a plot of the cohesion ratio L_{F_1}/L_{F_o} versus the ultrasonic amplitude ratio λ/λ_o. The curve shows a slight positive curvature similar to the plots of cohesion ratio versus compression ratio. Of significance in Fig. 28 is that the curve extrapolates through $L_{F_1}/L_{F_o} = 1.0$ for $\lambda/\lambda_o = 1.0$.

Plots of the cohesion stress and cohesion coefficient versus the ultrasonic wave amplitude ratio are given in Fig. 29. The curves are similar in form to those for cohesion stress and cohesion coefficient versus the compression ratio L_C/L_{F_o}.

Also included in Fig. 27 are the results for specimens exposed to O_2 for a sufficient exposure to have reduced the cohesion coefficient to 0.5 (Fig. 24). The ultrasonic amplitude ratio for these specimens is the same as that for those exposed to nitrogen, which exhibit a cohesion coefficient of about 0.90. This suggests that the ultrasonic measurements provide a measure of the area of contact independent of the degree of cohesion.

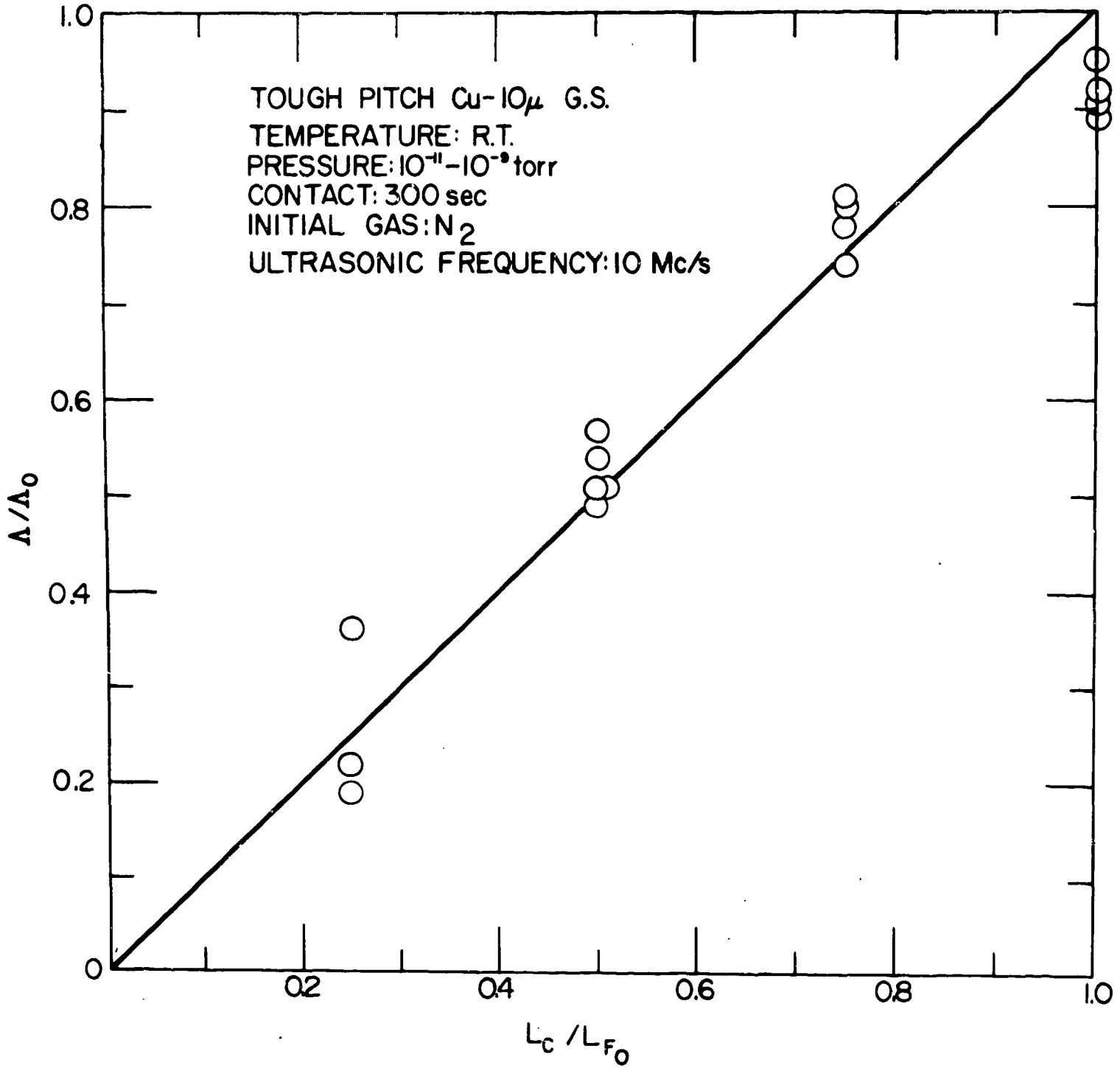

Fig. 26. Effect of Compression Ratio on the Ratio of the Amplitude of the Transmitted Ultrasonic Wave for a Cold Welded Specimen, λ, to that for a Virgin Specimen at Maximum Load, λ_o, for Annealed Tough Pitch Copper

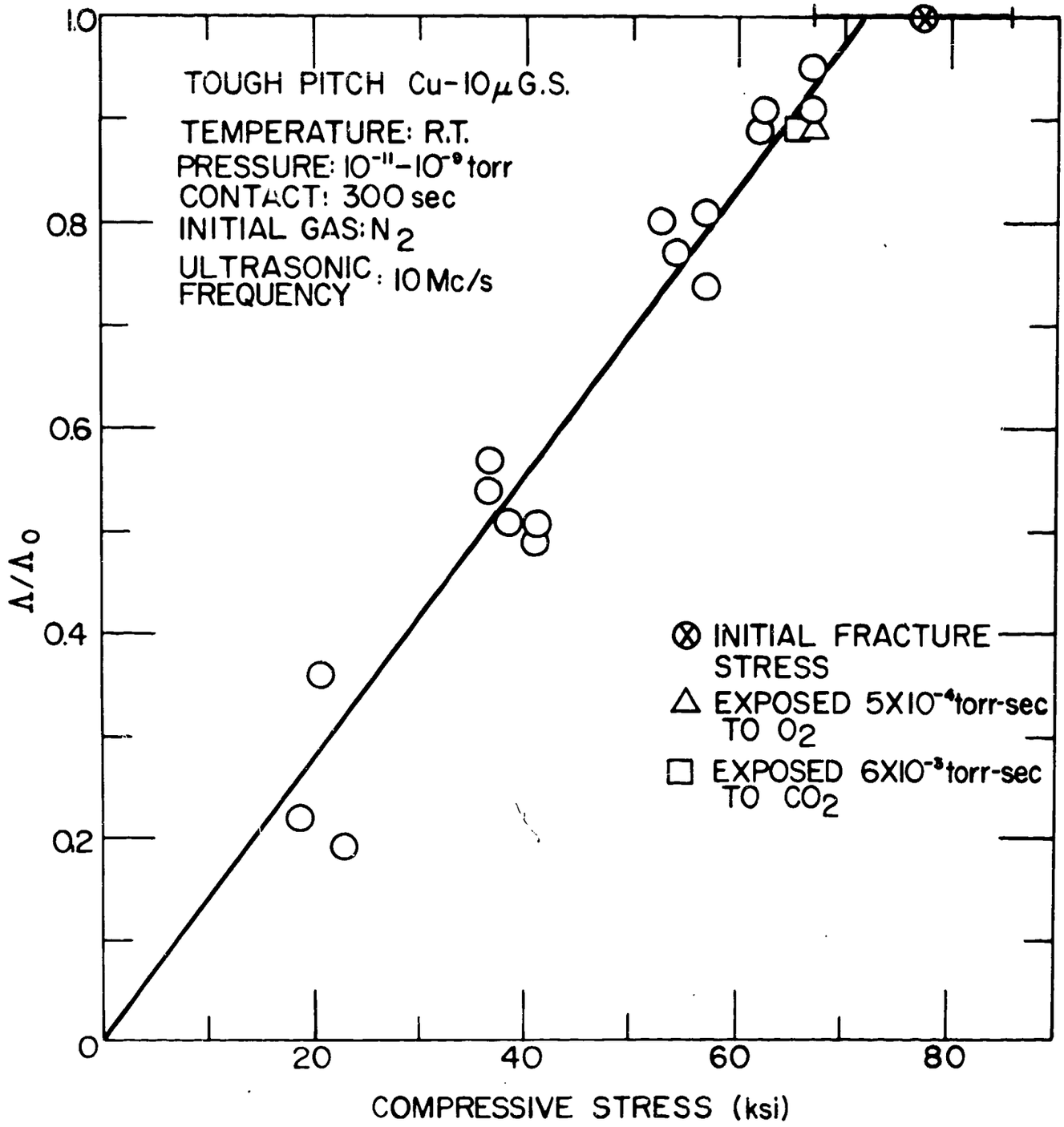

Fig. 27. Effect of Compression Stress on the Ratio of the Amplitude of the Transmitted Ultrasonic wave for a Cold Welded Specimen, λ, to that for a virgin Specimen at Maximum Load, λ_0, for Annealed Tough Pitch Copper

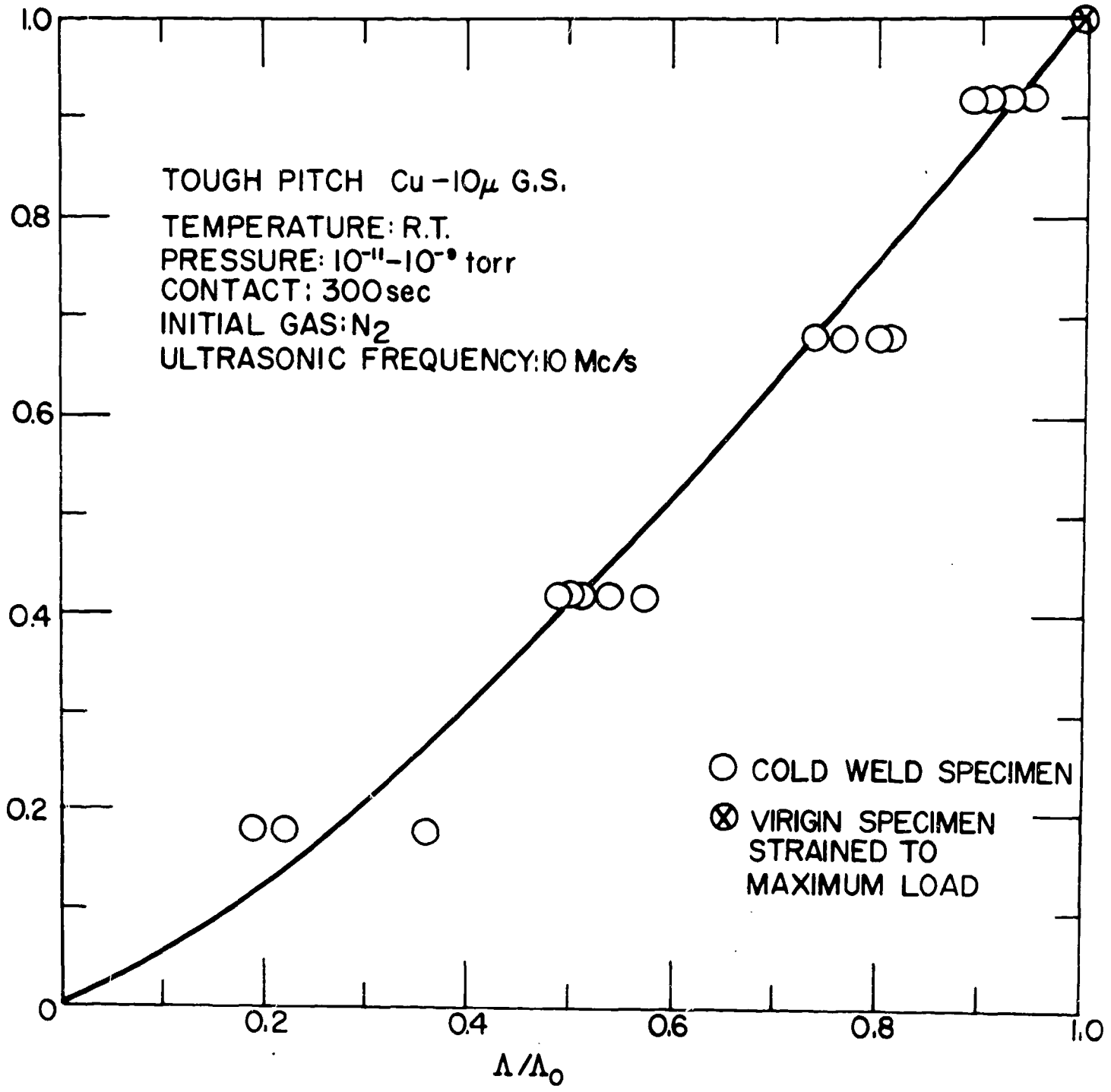

Fig. 28. Cohesion Ratio Versus Ultrasonic Amplitude Ratio for Annealed Tough Pitch Copper

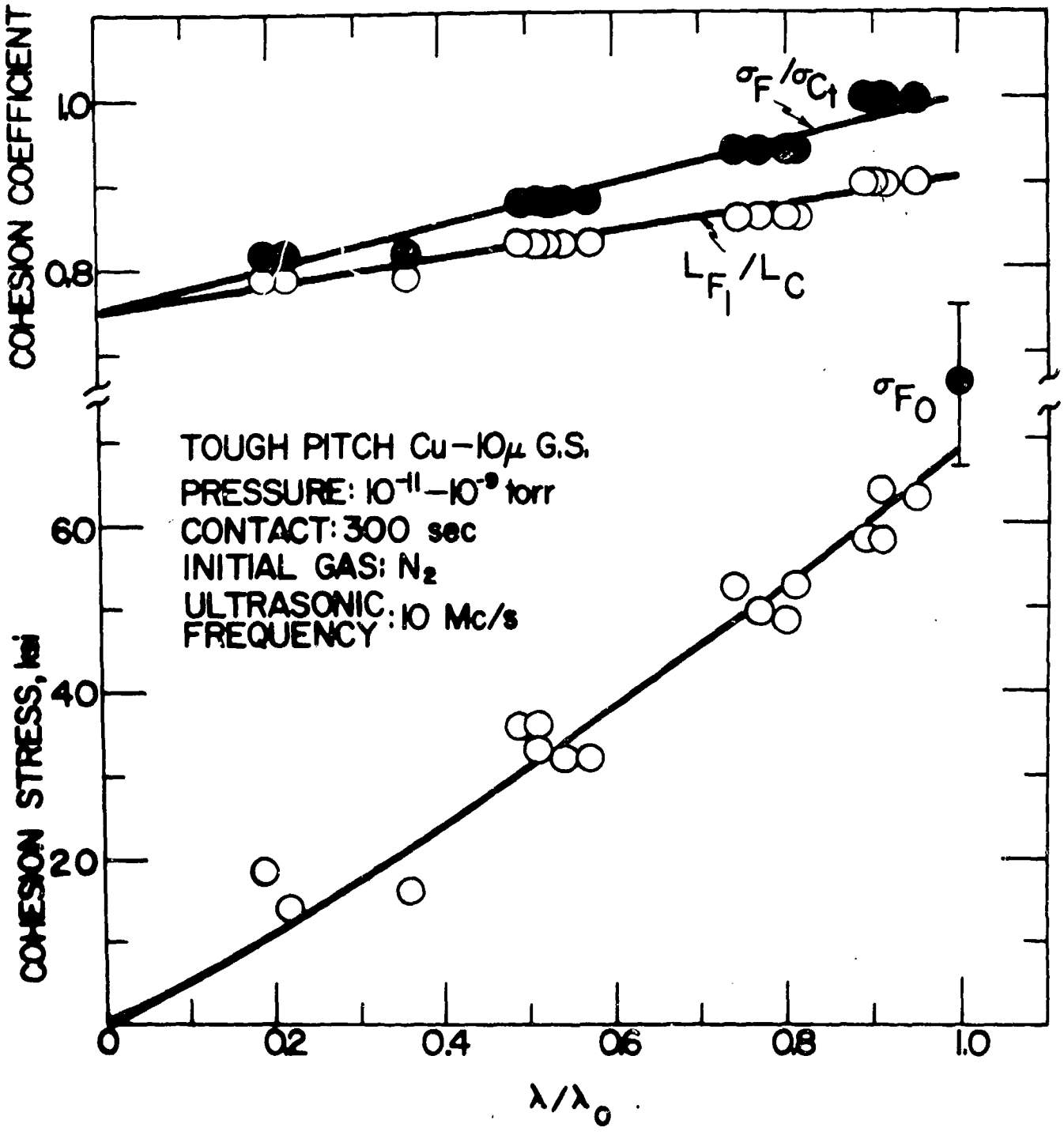

Fig. 29. Cohesion Coefficient and Cohesion Stress Versus Ultrasonic Amplitudes Ratio for Annealed Tough Pitch Copper.

3.5 Microscopic Studies

The appearance of the fracture surface of an annealed tough pitch copper specimen with a 10μ grain size is illustrated in Fig. 30. The fracture has a typical ductile fibrous character, providing a rather rough initial surface for the cold welding operation. Similar ductile fracture surfaces were observed for the other annealed materials investigated.

Detailed microscopic studies of the structure of the weld interface were only made for the copper specimens. The photomicrograph of Fig. 31 illustrates the appearance of the weld interface near the center of a cold welded annealed tough pitch copper specimen (10μ grain size) when viewed in the unetched condition. Porosity is noted along the weld interface for a compression ratio R_C = 0.5, while there is no indication of voids for R_C = 1.0 at the magnification shown or at higher magnifications (up to 1000 x). Porosity was always found for compression ratios less than 1.0, the amount increasing with decrease in R_C.

The appearance of the interface in fine-grained (6μ) OFHC specimens was similar to that for the annealed tough pitch copper described above. However, the coarse grained (100μ) OFHC and coarse-grained (450μ) high purity specimens exhibited some porosity even for R_C= 1.0; see, for example, Fig. 32.

Examples of the appearance of the weld interface after etching for R_C = 0.5 and R_C = 1.0 are shown in Figs. 33-38. Again, porosity is evident in the large grain size material at R_C = 1.0 and for all materials at R_C = 0.5. The excellent matching of the two fracture surfaces possible with the present apparatus is revealed in Fig. 36.

Comparing Figs. 37 and 38 with Fig. 36 indicates that the matching of the fractured surfaces did not occur as well for the more ductile OFHC copper specimens as for the tough pitch copper. That recrystallization may occur along the weld interface during the joining of cold worked specimens is indicated in Figs. 39 and 40. The recrystallized zone is much

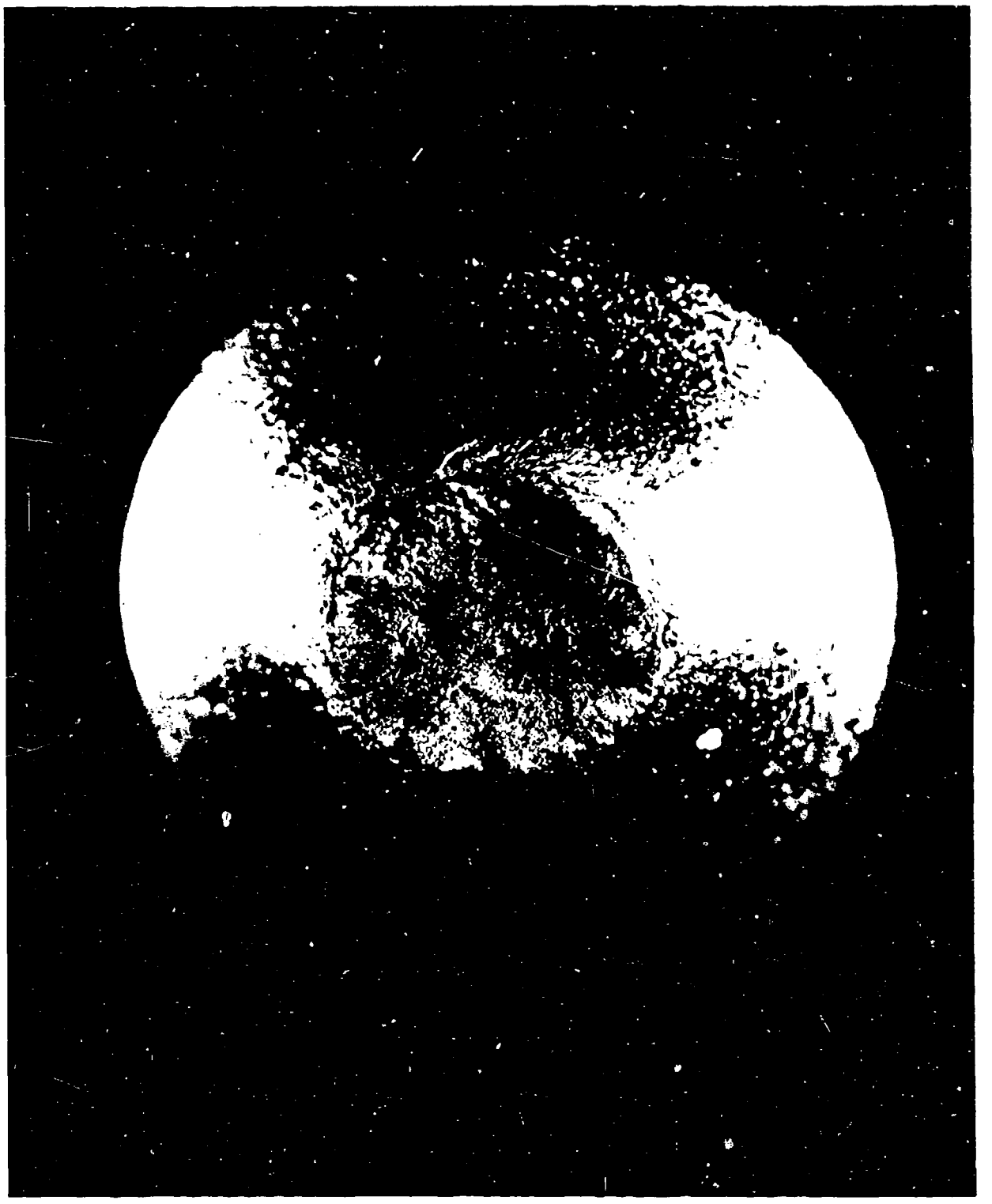

Fig. 30. Enlarged Views of the Fracture Surface of Annealed Tough Pitch Copper of 10μ Grain Size

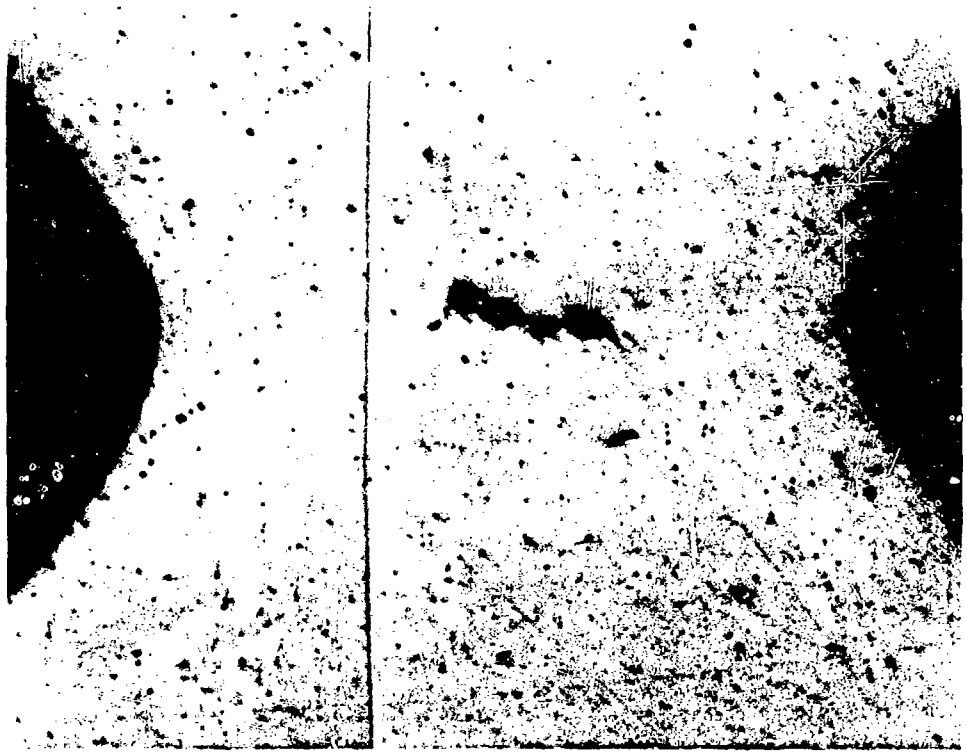

(a)

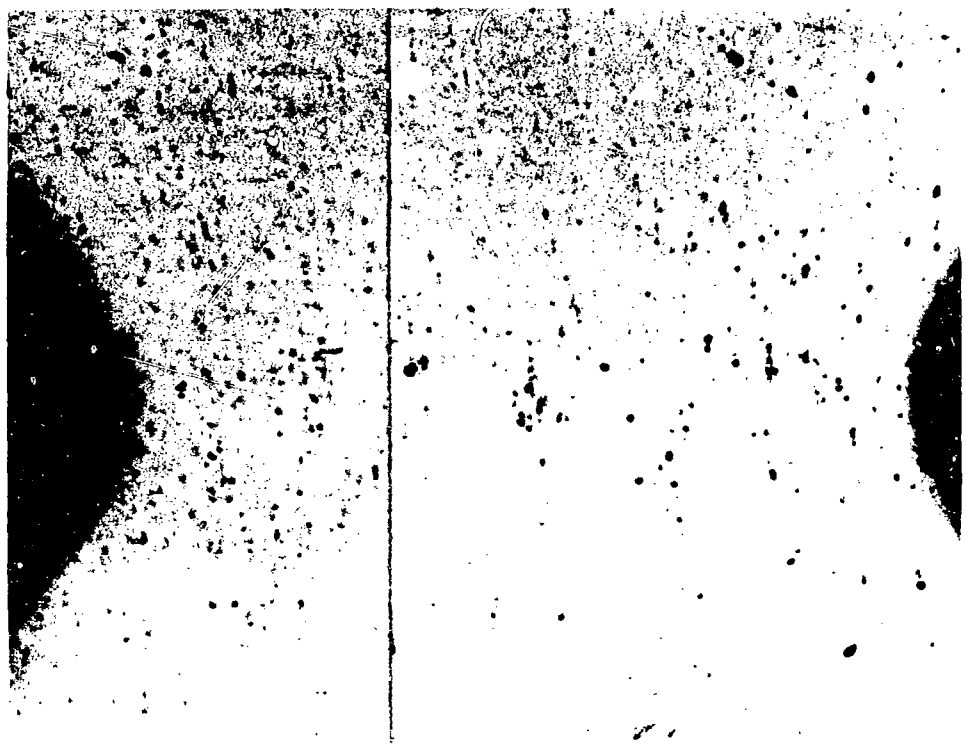

(b)

Fig. 31. Unetched Cross-Section of Cold Welded Annealed Tough Pitch Copper of 10μ Grain Size (a) L_C/L_{F_o} = 0.5 (b) L_C/L_{F_o} = 1.0 Orig. Mag. 60x

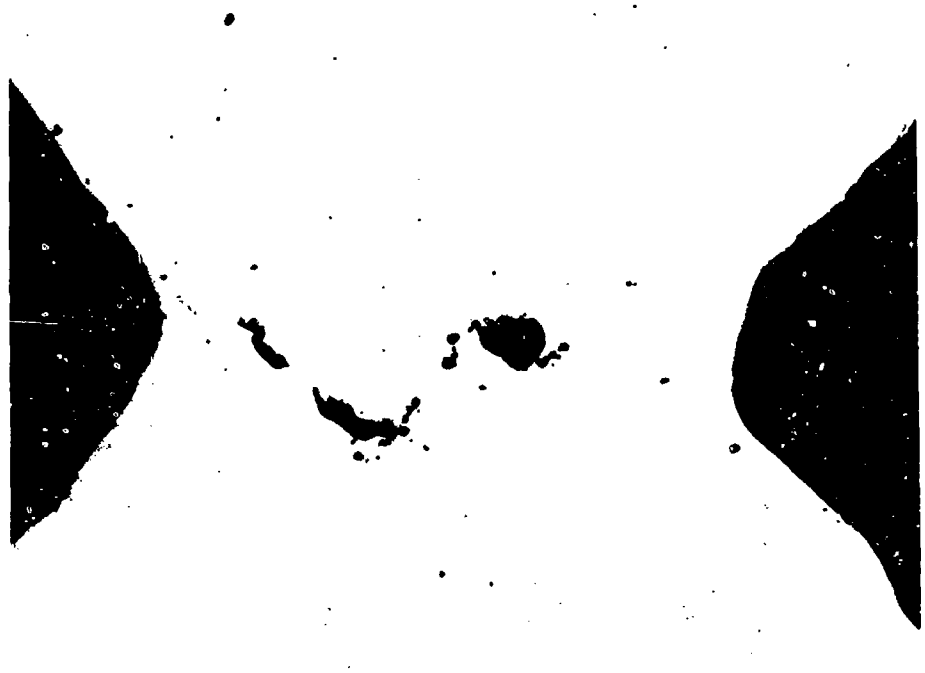

(a)

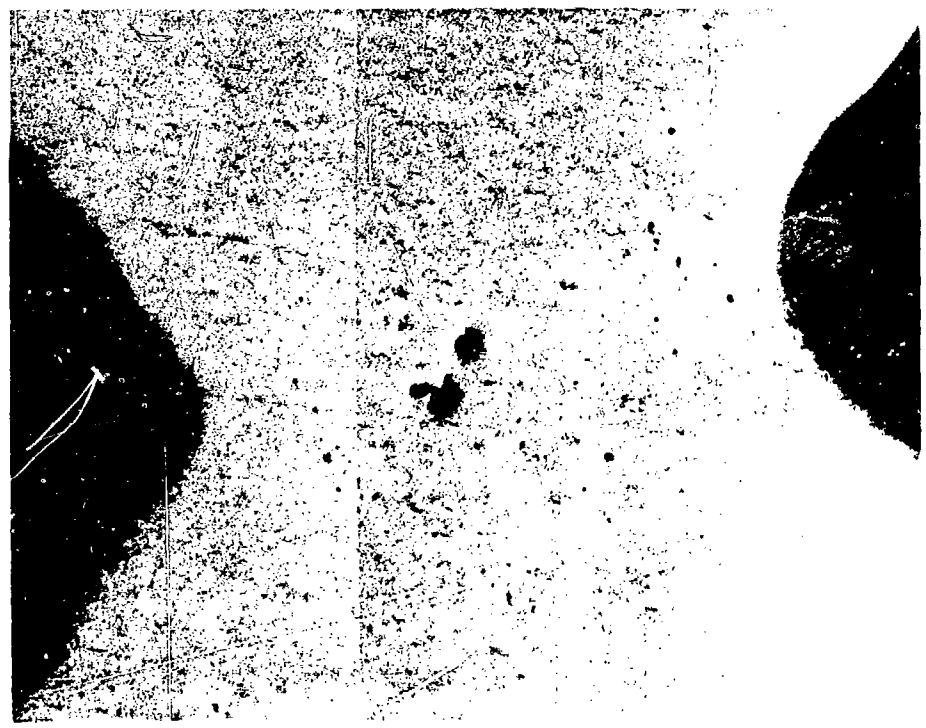

(b)

Fig. 32. Unetched Cross-Section of Cold Welded OFHC Copper of 100μ Grain Size (a) L_C/L_{C_o} = 0.5 (b) L_C/L_{F_o} = 1.0 Orig. Mag 60x

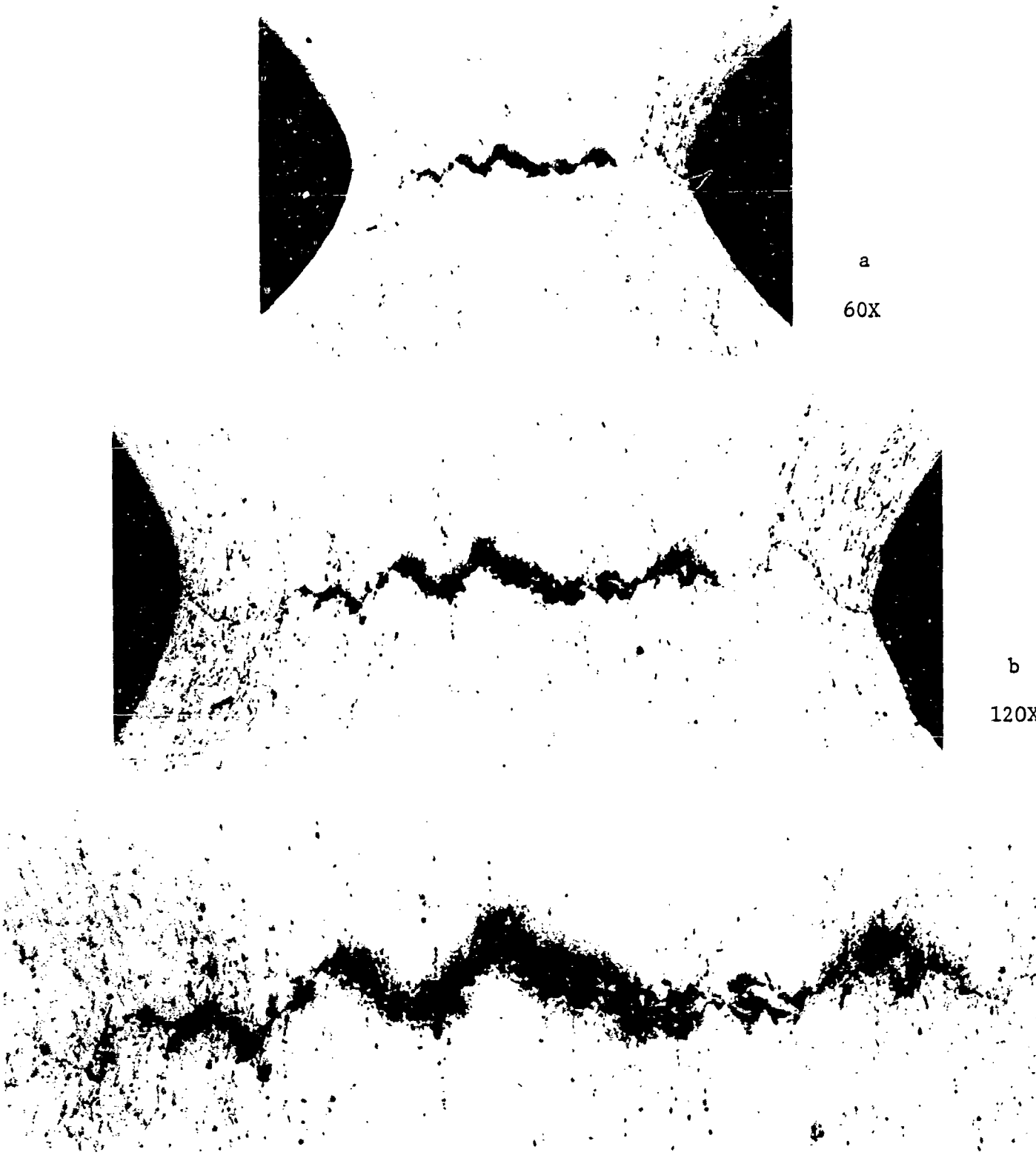

Fig. 33. Microstructure of the Weld Interface for Annealed Tough Pitch Copper of 10μ Grain Size for L_C/L_{F_o} = 0.5

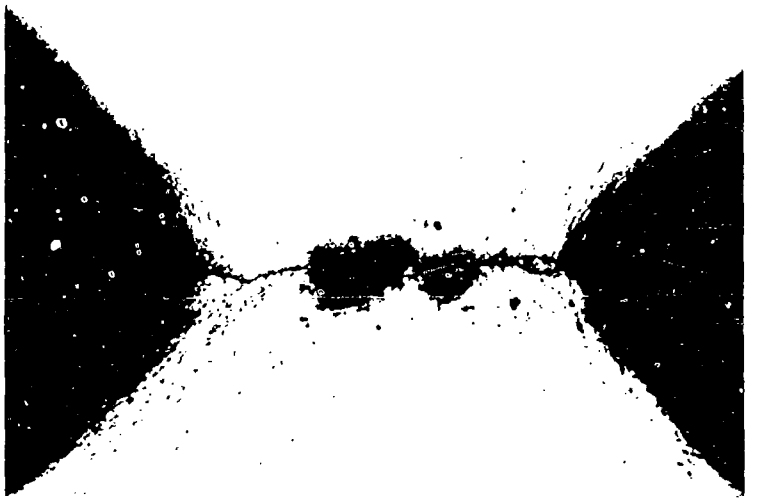

60X

120X

240X

Fig. 34. Microstructure of the Weld Interface for Annealed OFHC Copper 7μ Grain Size for L_C/L_{F_o} = 0.5

60X

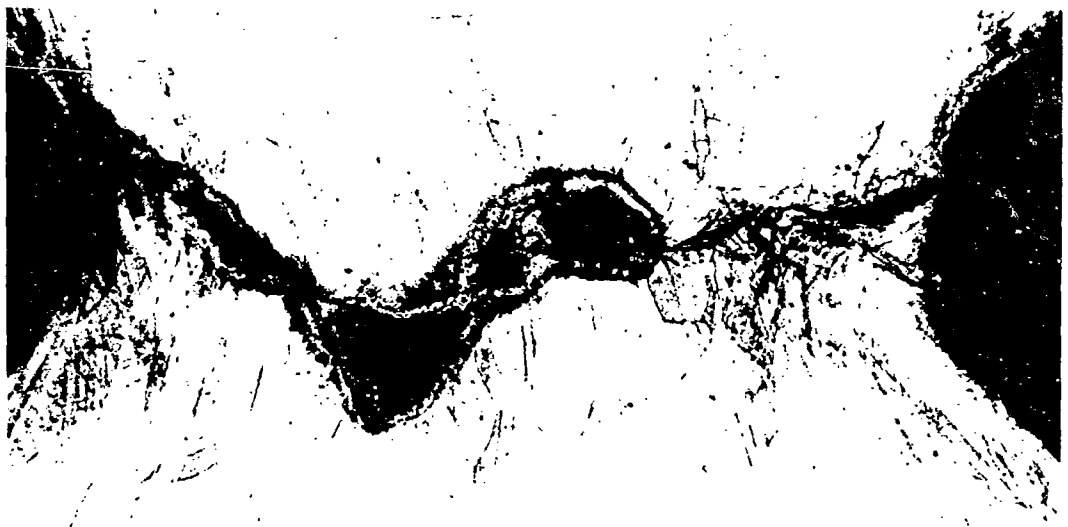

120X

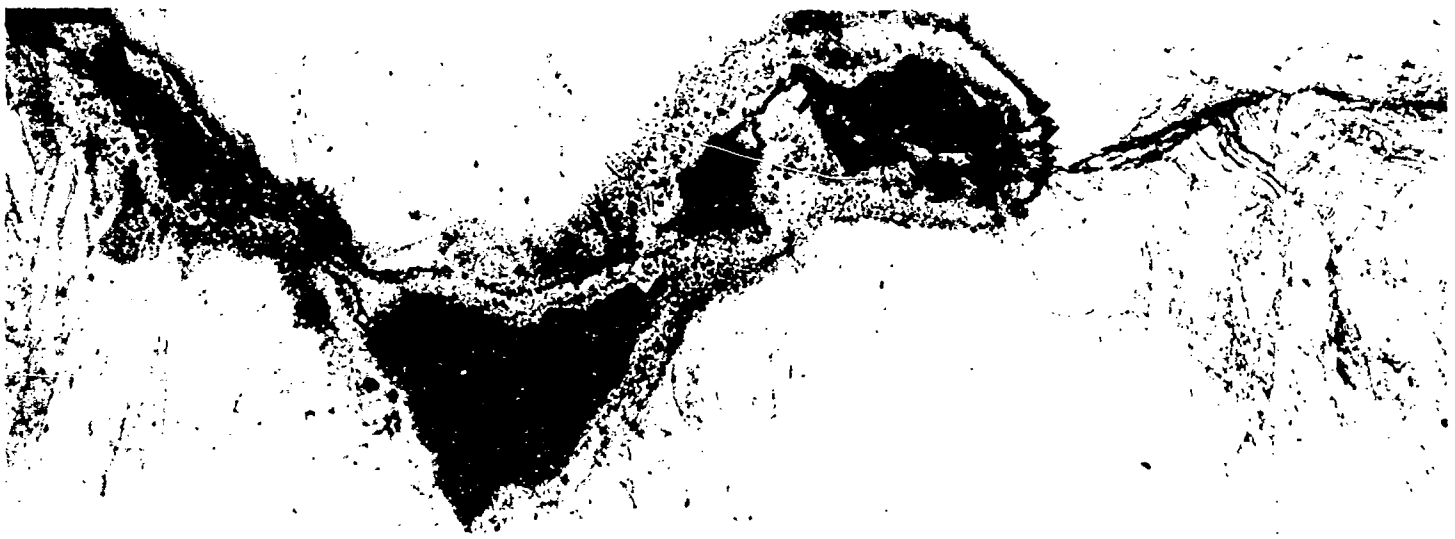

240X

Fig. 35. Microstructure of the Weld Interface for OFHC Copper of 100μ Grain Size for L_C/L_{F_O} = 0.5

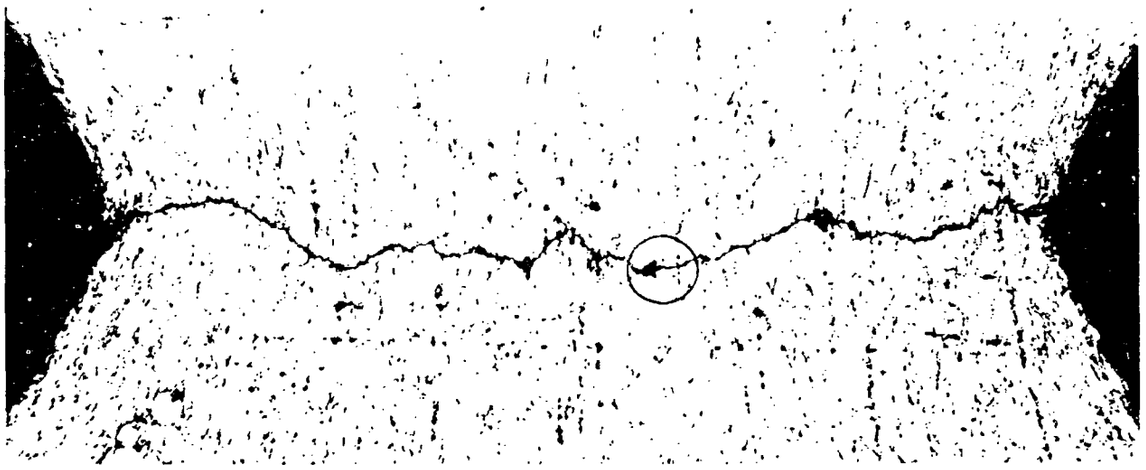

120X

960X

Fig. 36. Microstructure of the Weld Interface for Annealed Tough Pitch Copper of 10μ Grain Size for L_C/L_{F_0} = 1.0

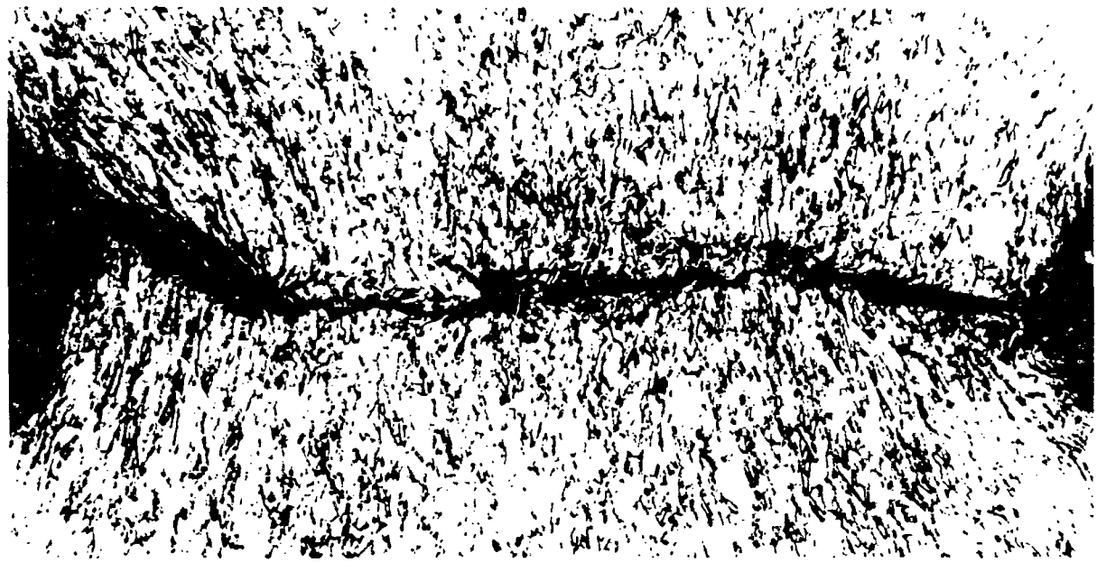

120X

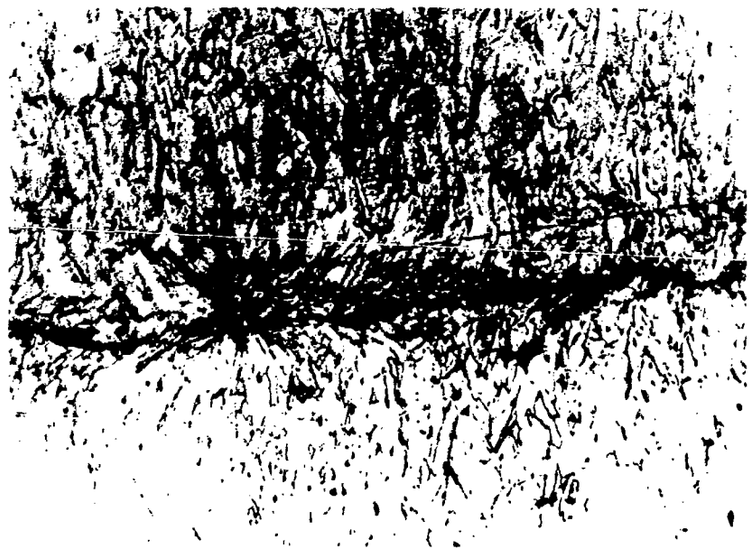

240X

Fig. 37. Microstructure of the Weld Interface for Annealed OFHC Copper of 7μ Grain Size for L_C/L_{F_o} = 1.0

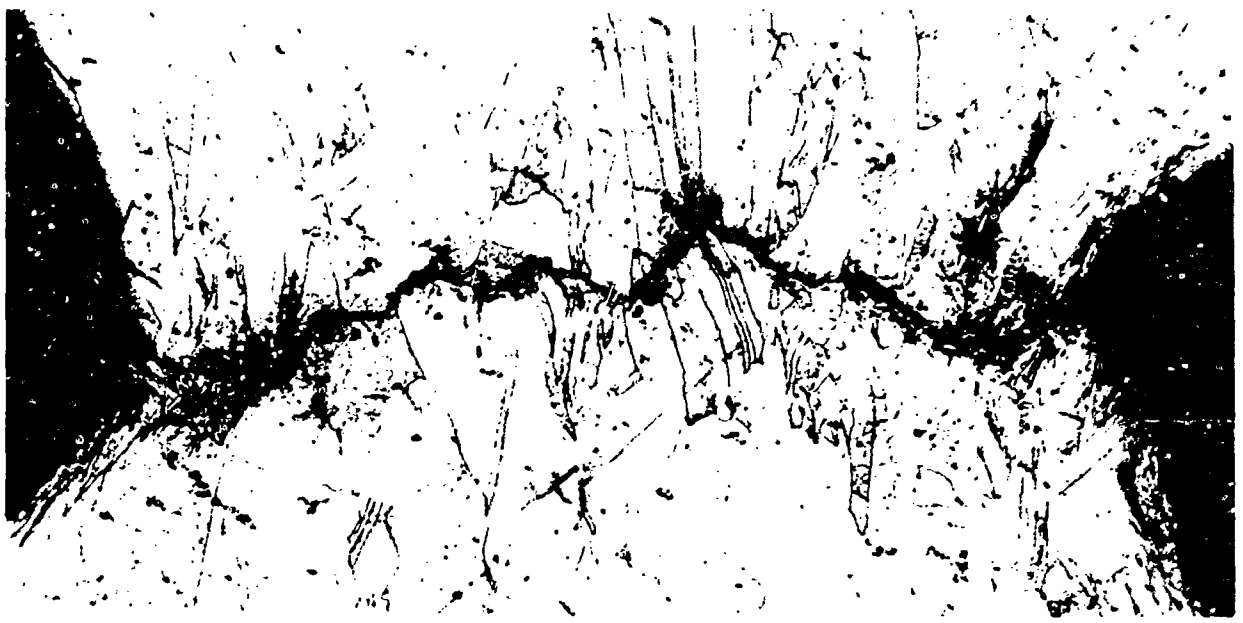

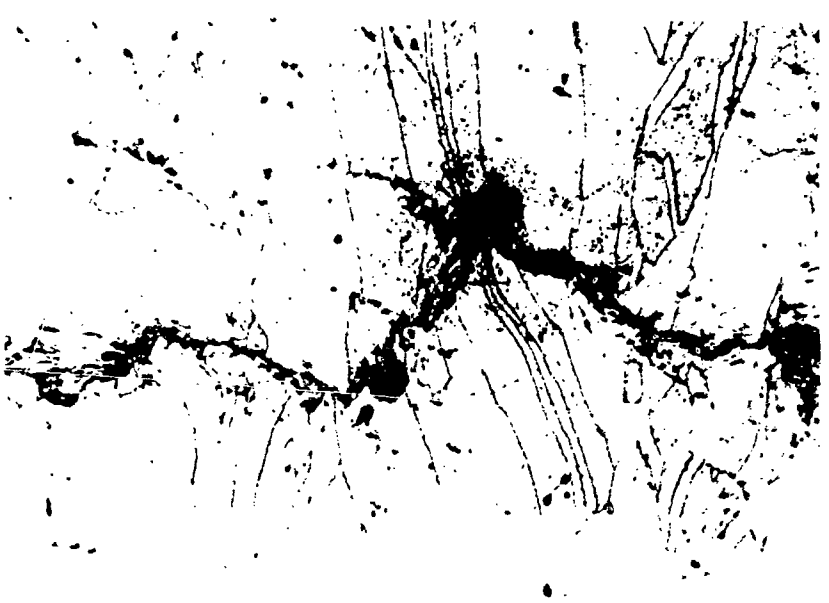

Fig. 38. Microstructure of the Weld Interface for Annealed OFHC Copper of 100μ Grain Size for L_C/L_{F_o} = 1.0

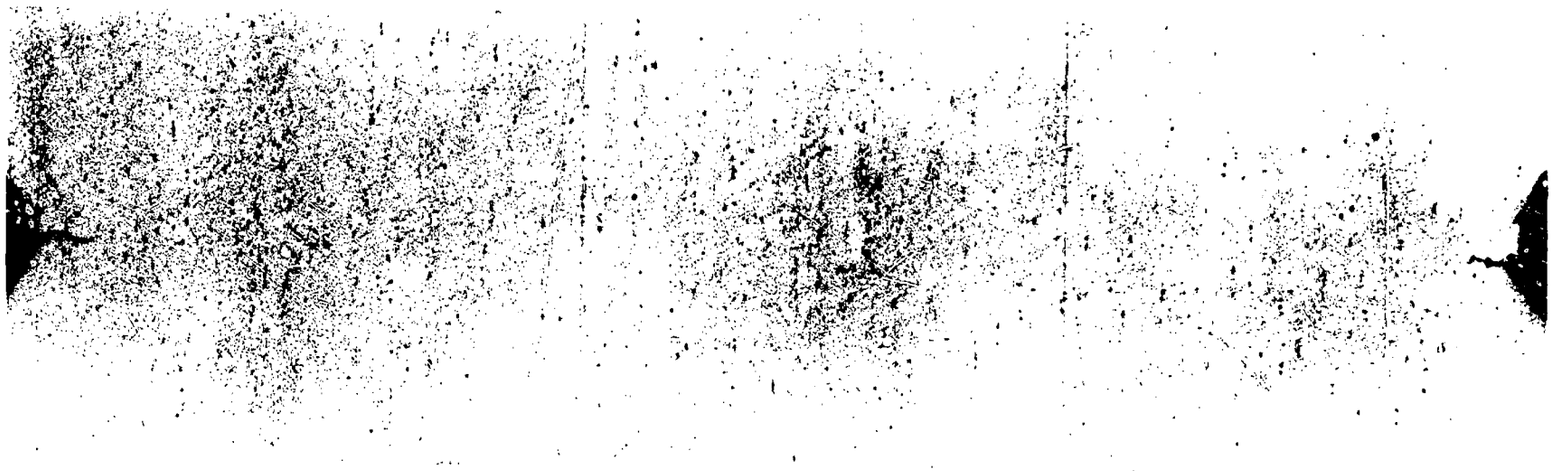

a as polished 120X

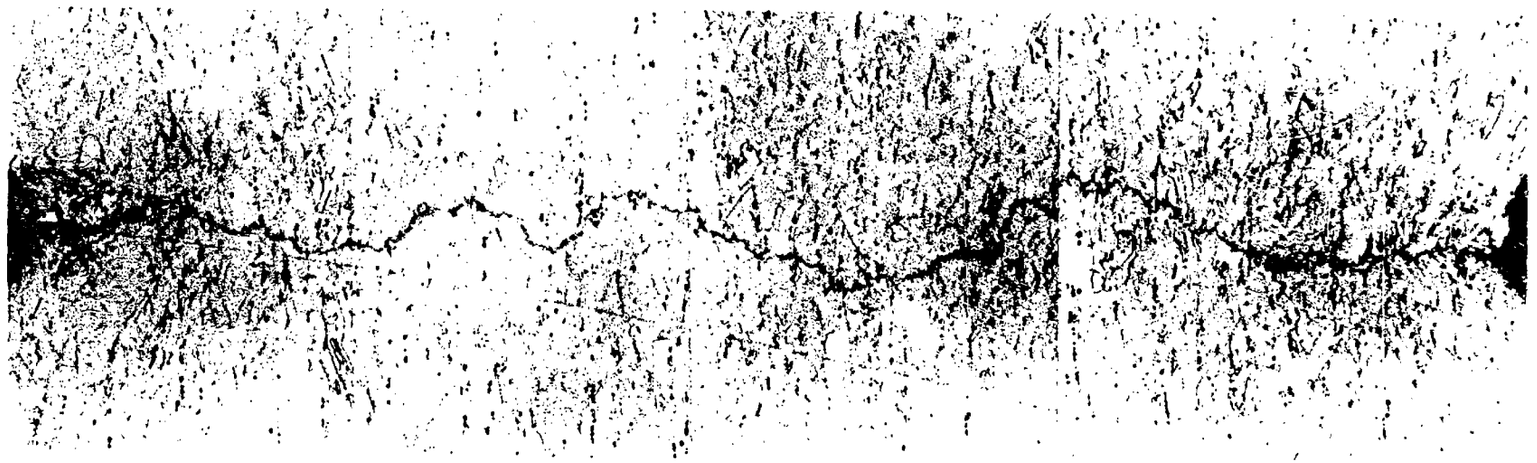

b as etched 120X

Fig. 39. Microstructure of the Weld Interface for Cold Worked Tough Pitch Copper Indicating Recrystallization at the Interface; L_C/L_{F_o} = 1.0 (a) As-Polished (b) Etched Orig. Mag. 120x

a as polished 120X

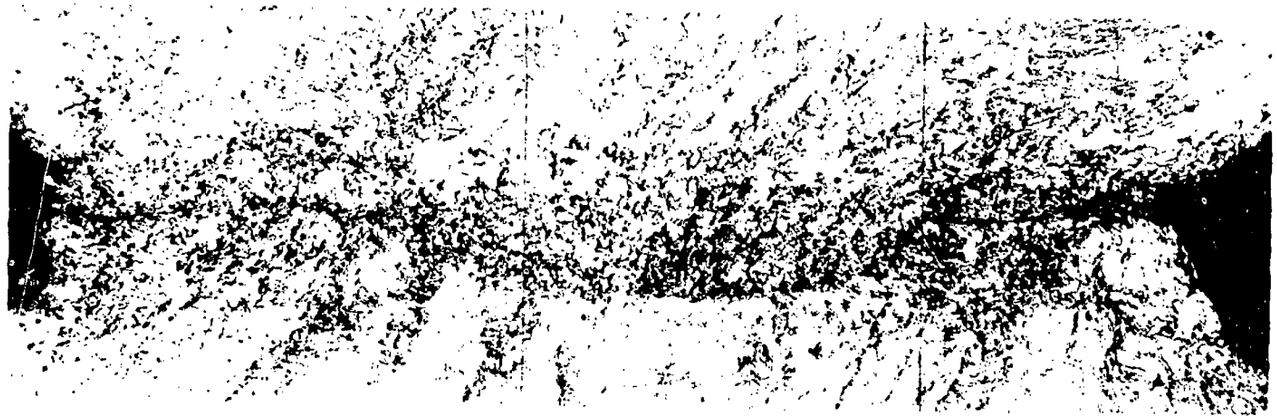

b as etched 120X

Fig. 40. Microstructure of the Weld Interface for Cold Worked High Purity Copper Showing Recrystallization at the Weld Interface; L_C/L_{F_O} = 1.0 (a) As-Polished; (b) Etched Orig. Mag. 120x.

wider in the high purity copper as compared to the tough pitch copper, being only faintly visible in the latter material.

3.6 Effect of Heat Treatment

A very limited study was made on the effect of a subsequent heat treatment (1 hour at 300°C and 1 hour at 600°C in a vacuum of 10^{-6} torr) on the strength of the weld for tough pitch copper with a 10μ grain size. The results are summarized in Table IV. The cohesion coefficient $\alpha = L_{F_1}/L_C$ was reduced by both heat treatments, the higher temperature producing the greater effect. This was surprising for it was hoped that the annealing treatment would improve the cohesive strength by removing internal stresses and by promoting sintering. Consequently, a metallographic examination was made of the weld interface following the heat treatment. The structures observed are presented in Figs. 41 and 42. In Fig. 41 it is seen that the annealing treatment of 1 hour at 300°C only recrystallized the material in the immediate vicinity of the interface without noticeably affecting the structure away from the interface. The heat treatment of 1 hour at 600°C produced recrystallization in the entire notched region of the specimen, leading to a refinement of the grain size in this region. In this case the original weld interface is only faintly discernable through the existence of a finer grain size along its path. In neither figure is there any indication that the annealing treatment caused any deterioration along the weld interface.

Table IV. Effect of Subsequent Heat Treatment on the Strength of the Cold Weld in Tough Pitch Copper with 10μ Grain Size

Spec.	Heat Treatment	Compression Ratio	Cohesion Coefficient
73	1 hr. @300°C	L_C/L_{F_o}	L_{F_1}/L_C
70	1 hr. @600°C	1.0	0.72
71	1 hr. @600°C	1.0	0.53

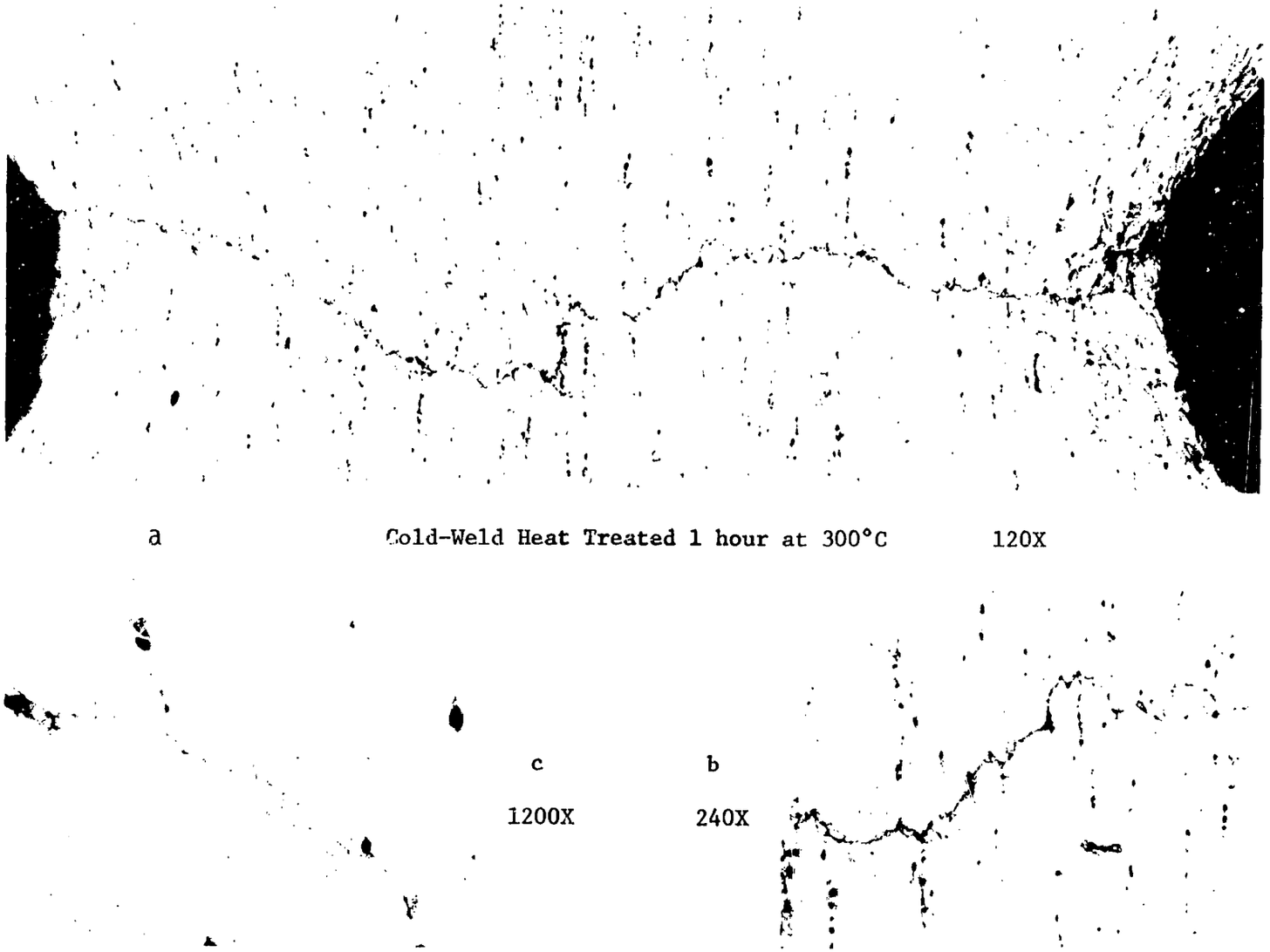

Fig. 41. Microstructure of the Weld Interface for Annealed Tough Pitch Copper of 10μ Grain Size After a Heat Treatment of 1 hour at 300°C. L_C/L_{F_O} = 1.0 (a) 120x; (b) 240x; (c) 1200x.

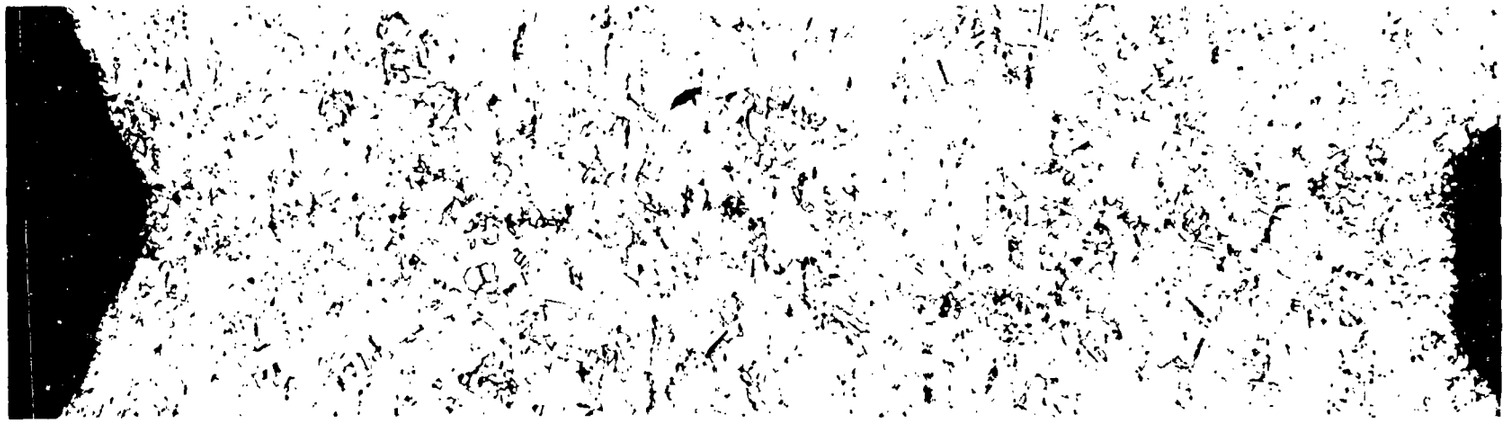

a 120X

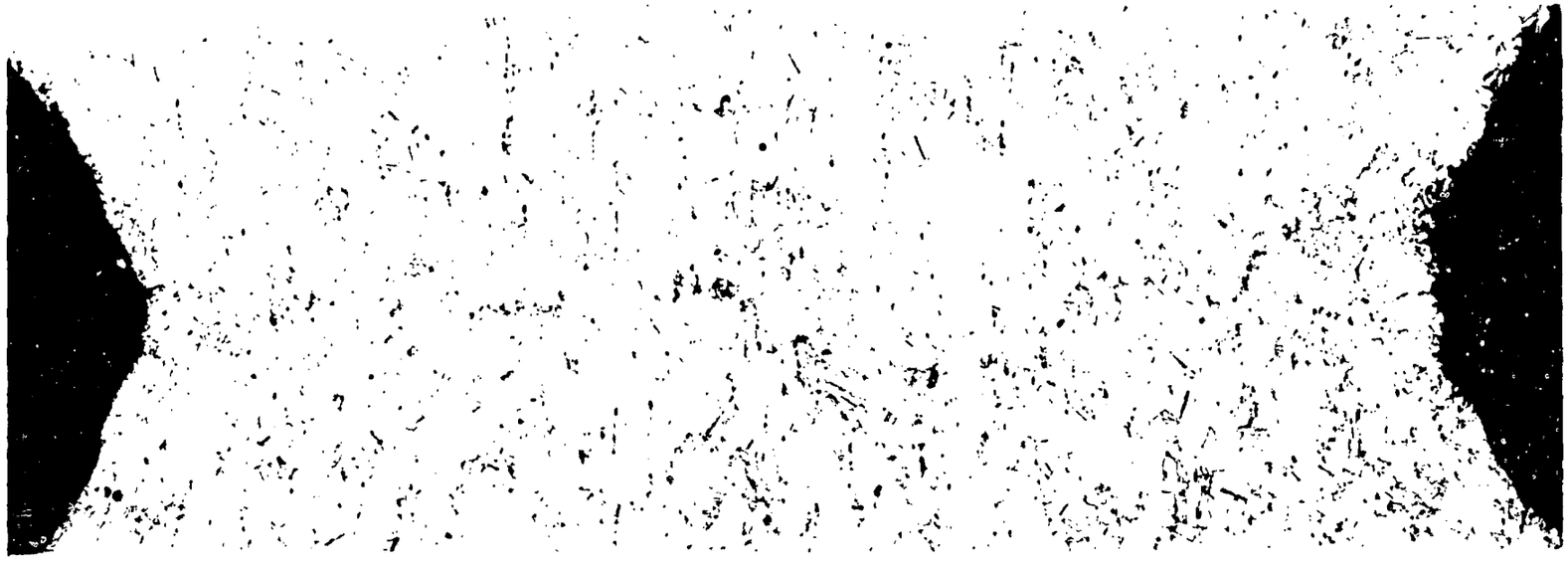

b 240X

Fig. 42. Microstructure of the Weld Interface for Annealed Tough Pitch Copper of 10μ Grain Size After a Heat Treatment of 1 hour at 600°C. L_C/L_{F_o} = 1.0 (a) 120x; (b) 240x.

4. DISCUSSION

4.1 Cohesion Under Ultrahigh Vacuum

4.1.1 Unalloyed FCC Metals

The present study has established that reproducible results can be obtained with the technique of using fractured specimens for studying the cohesion of ductile metals and that the results from such studies can yield significant information. The technique as employed here has, however, two distinct limitations: (1) the material to be joined has been deformed to fracture prior to the initiation of the cohesion test and (2) the surface profile or geometry is invariably that corresponding to a ductile fracture. It is therefore important to compare the cohesion results obtained in the present investigation with those of other investigators using the same technique or other techniques. Available data are summarized in Table V. It is here seen that there is surprisingly good agreement in the value of the cohesion coefficient α obtained by the various investigators using different techniques and different surface conditions, with α ranging from about 0.60 to 1.15. Thus it appears that the cohesion coefficient is not sensitively dependent on the technique employed or the surface geometry. The most critical factor appears to be the cleanliness of the surface, as indicated in the present investigation and previously (8), (9).

A most significant finding of the present investigation is that the cohesion results for all of the unalloyed FCC metals considered can be normalized to a single curve through the original fracture load or the original fracture stress of the virgin specimens. Considering the ultrasonic measurements and microscopic observations along with the cohesion results, one is led to the conclusion that the original fracture strength governs both the area of contact developed during the compression loading and the subsequent cohesive strength of the bond.

TABLE V. COMPARISON OF COHESION RESULTS FOR FCC METALS AND BRASS

Metal	Ref.	Surface Profile	Surface Preparation	Contact Pressure: Vacuum torr	Contact Pressure: Load Xg	Contact Pressure: Stress Kg/mm^2	Cohesion Coefficient L_{F_1}/L_C
A1(99.99)	1	Ductile Fracture (d_o = 1.25 cm)*	As-Fractured	5×10^{-10}	45	--	0.84
A1(1100)	Present	Ductile Fracture (d_o = 0.25 cm)*	As-Fractured	$10^{-11} - 10^{-9}$	10-39	13-56	0.77-0.85
Ag	2	Crossed 1 mm wires	Argon Bombard	10^{-10}	0.0057	--	0.84
Ag(99.9+)	1	Ductile Fracture (d_o = 1.25 cm)*	As-Fractured	5×10^{-10}	45	--	0.78
Ag(99.9+)	Present	Ductile Fracture	As-Fractured	10^{-11}-10^{-9}	10-62	19.72	0.78-0.89
Cu(OFHC)	3	Hemisphere (d_o=1 cm) on Flat (d_o=102 cm)	Electropolish and Electron Bombard	10^{-11}	0.050	--	1.00
Cu(OFHC)	4	Hemisphere (d_o=1.9 cm) on cylinder	Machine to 8 RMS dip in 20% HNO_3.	10^{-11}	0.360	66	1.00**
Cu(OFHC)	5, 6	Ductile Fracture (d_o=?)*	As-Fractured	5×10^{-10}	--	39	0.66-1.15
Cu(OFHC)	1	Ductile Fracture (d_o=1.25 cm)*	As-Fractured	5×10^{-10}	45	--	0.78
Cu	Present	Ductile Fracture	As-Fractured	10^{-11}-10^{-9}	5-285	2-128	0.62-0.98
Ni (99.5+)	Present	Ductlle Fracture (d_o=0.25 cm)*	As-Fractured	10^{-11}-10^{-9}	35-206	51-116	0.73-0.87
Cu70Zn30	Present	Ductile Fracture (d_o=0.25 cm)*	As-Fractured	10^{-11}-10^{-9}	40-119	22-72	0.46-0.59
Cu60Zn40	1	Ductile Fracture	As-Fractured	5×10^{-10}	45	--	0.11

TABLE V. COMPARISON OF COHESION RESULTS FOR FCC METALS AND BRASS (Cont'd)

References:

1. W. P. Gilbreath-ASTM STP 431 *Adhesion or Cold Welding of Materials in Space Environments* p 128 (1967).
2. D. V. Keller - *Surfaces and Interfaces I,* Sycracuse Univ. Press. p. 225 (1967).
3. D. H. Buckley - *Adhesion or Coiewelding of Materials in Space Environments,* ASTM STP 431 p. 248 (1967).
4. J. S. Przybyszewski - "Stress-Strain Behavior of Coldwelded Copper Microjunctions in Vacuum As Determined from Electrical Resistance Measurements", NASA TN d-4743 (Aug. 1968).
5. J. L. Ham-ASLE Trans 6 20 (1963).
6. J. L. Ham - "Cohesion of Copper and Steel Repeated Fractured and Rejoined in Vacuum" ASE 632D (Jan 14-18 1963).

Notes:

* Notched tensile specimen

** Based on actual contact area

Of the various mechanical property phenomena, the fracture of ductile metals is among those least understood. This in large part due to the fact that the fracture strength is sensitively dependent not only on the stress state but also on the structure (microstructure and crystalline defects) which is initially present and which develops during the straining to the point of fracture. The effects of such fundamental crystal properties as elastic modulus, surface energy, stacking fault energy, etc. on the fracture strength are usually completely overshadowed by the variations in structure which may exist. This is evident if one compares the original fracture stresses of the various metals in Table II. Therefore, it seems pointless to attempt to interpret the cohesion of such materials in terms of fundamental physical properties unless the stress state and the structure existing at the time of fracture of the bond are clearly identified and their influence established. Consequently, the approach here will be to interpret the cohesion results in terms of the fracture stress rather than in terms of fundamental physical properties. In keeping with modern concepts of ductile fracture, the fracture stress will be considered to be a point on the flow stress versus strain curve.

Initially let us consider the effect of the compressive load on cohesion. Taking the amplitude of the ultrasonic wave to be proportional to the area of intimate contact A_c across the weld interface, the results of the ultrasonic measurements in Figs. 26 and 27 indicate that A_c is directly proportional to the ratio of the "average" compression stress $\overline{\sigma}_{F_o}$; i.e.

$$\frac{\lambda}{\lambda_o} = \frac{A_c}{A_{F_o}} = K \frac{L_C}{L_{F_o}} = K' \frac{\overline{\sigma}_C}{\sigma_{F_o}} \qquad (4)$$

where K and K' are constants of the order of unity. If we now make the assumption that the fracture of the bond occurs at a constant true fracture stress, given by σ_{F_o}, then

$$\frac{\overline{\sigma}_{F1}}{\sigma_{F_o}} = \frac{A_c}{A_{F_o}} = K \frac{L_C}{L_{F_o}} = K' \frac{\overline{\sigma}_C}{\sigma_{F_o}} \tag{5}$$

and

$$\frac{L_{F1}}{L_{F_o}} = K \frac{L_C}{L_{F_o}} \tag{6}$$

and K (or K') becomes the cohesion coefficient α.

The results of Figs. 16 and 21 show that Eq. 5 and 6 are closely approximated with K and K' = 0.9-1.0 for values of L_C/L_{F_o} $(\overline{\sigma}_C/\sigma_{F_o})$ greater than about 0.5. For L_C/L_{F_o} $(\overline{\sigma}_C/\sigma_{F_o}) \leq 0.5$, K(K') varies with the compression ratio L_C/L_{F_o} $(\overline{\sigma}_C/\sigma_{F_o})$, decreasing with decrease in compression ratio and becoming approximately 0.75 for L_C/L_{F_o} $(\sigma_C/\sigma_{F_o}) = 0$.

In an earlier, preliminary consideration (10) it was felt that the effect of compressive load on α reflected the fact that the area of contact A_c was a parabolic function of the compression stress. The additional ultrasonic measurements made since that time indicate that this is not the case, but rather that A_c is proportional to the stress. The observed variation of α with stress may then be due to the stress concentrations associated with the presence of the voids along the interface. Eq. 5 should then be written

$$q \frac{\overline{\sigma}_{F1}}{\sigma_{F_o}} = \frac{A_c}{A_o} = K' \frac{\overline{\sigma}_C}{\sigma_{F_o}} = K \frac{L_C}{L_{F_o}} \tag{7}$$

where q represents the average stress concentration factor or plastic constraint factor. Rearranging Eq. 7 gives

$$\frac{\overline{\sigma}_{F1}}{\sigma_{F_o}} = \frac{K'}{q} \frac{\overline{\sigma}_C}{\sigma_{F_o}} \tag{7a}$$

and taking $\frac{K'}{q}$ as α and substituting Eq. 1 for α one obtains

$$q = \frac{K'}{\alpha_o + \beta\ (\bar{\sigma}_C/\sigma_{F_o})} = \frac{K'}{\left(\alpha_o + \frac{\beta}{K'}\frac{A_c}{A_o}\right)} \tag{8}$$

Eq. 8 yields for $\bar{\sigma}_C/\sigma_{F_o} = 0.5, K' = 1.0$, $q = 1.32$, which is reasonable considering the size and shape of voids observed along the interface, Figs. 33-40.

Also of significance in regard to the cohesion results is that all the data fell on one curve for a plot of "average" cohesive stress versus "average" compression stress. This feature follows directly from Eq. 7 which gives

$$\bar{\sigma}_{F_1} = \frac{K'}{q}\,\bar{\sigma}_c \tag{9}$$

Thus, although the area of contact is less at a given compression stress for a metal of higher fracture stress, the strength of the bond is also higher, thereby yielding a constant cohesion strength.

4.1.2 Cu70Zn30 Alloy

The lower cohesion of the 70-30 brass specimens as compared to the unalloyed FCC metals is not understood at this time. One possibility is that during the joining of the two fractured halves, any short range order which existed across the interface just prior to fracture was not re-established, thereby yielding an appreciably lower surface energy across the interface. Another possibility is suggested by the observation that the pressure in the vacuum system generally increased by an order of magnitude at the instant of initial fracture of the virgin specimen, suggesting the release of zinc vapor. It may be that some of this vapor recondensed onto the fractured surface, giving a lower bond strength. Time did not permit further evaluation of these speculations. Finally, it should be noted that a low cohesion coefficient was also observed for 60-40 brass by Gilbreath (9); see Table V.

4.1.3 Effect of Heat Treatment

The reduction in the cohesive strength which occurred upon heat treating the cold welded copper specimens is also not well understood at this time. As indicated earlier, there was no microscopic evidence of deterioration along the boundary, the only change being that recrystallization had occurred. This suggests that the lower cohesive strength after heat treatment may be due to a lower fracture strength of the recrystallized structure some support for which is suggested by the initial future loads in Figs. 6 and 7. If this is so, then the tendency for the cohesion of the cold worked specimens to exhibit a lower cohesive strength may be partly due to the recrystallization which occurred during the joining operation (Figs. 39 and 40). Again, time did not permit investigating this question in more detail.

4.2 Effect of Environment

4.2.1 Tensile Properties

The equality in strength values for all the metals considered here between the tests in N_2 at 760 torr and those in ultrahigh vacuum is not surprising, since at room temperature N_2 does not adsorb on any of these metals (11) and hence the surface condition in N_2 environment is expected to be equivalent to that in the ultrahigh vacuum. The slightly higher strengths obtained for Cu tested in CO, CO_2, O_2 and air must then be due to the fact that these gases are either strongly physiadsorbed or chemiadsorbed on the metal surface (11). The effect of such adsorbed gases may be to either hinder the egress of dislocations through the surface or inhibit the operation of dislocation sources at the surface. Comparing the mechanical strength values of Fig. 25 with the heats of adsorption in Table III, the effect of the environment appears to depend more on whether or not adsorption occurs than on the chemical strength of the adsorption. Worthy of mention is that higher strengths have also been observed for Al tested in ambient air as compared to vacuum (12, 13).

4.2.2 Cohesion

From adsorption rate theory (11) one can calculate the surface coverage N (molecules/cm^2) after exposure to a gas at a pressure P (dynes/cm^2) for a time t (seconds). For less than a monolayer of adsorption one obtains (14)

$$N = s\,\nu t\,[1-\exp.\,(-t/\tau)] \qquad (10)$$

where s is the sticking coefficient, $\nu = (P/2\,\pi m\,k\,T_g)^{1/2}$ is the number of molecules of gas with mass m striking the surface per second at gas temperature T_g and $\tau = \tau_o \exp\,(\Delta H_a/RT_s)$ is the mean time of residence of the gas on the surface. τ_o is the vibrational period of the surface atoms of the adsorbent and is usually about 10^{-13} second and ΔH_a is the heat of adsorption of the gas on the surface at temperature T_s. For a weakly adsorbed gas (low ΔH_a or long t) Eq. 10 reduces to

$$N_e = s\nu\tau = 3.5 \times 10^{22}\ \ s\,P\,\tau(MT_g)^{-1/2} \qquad (11)$$

while for a strongly adsorbed gas (high ΔH_a or short t).

$$N = s\nu\tau = 3.5 \times 10^{22}\ \ s\,Pt\,(MT_g)^{-1/2} \qquad (12)$$

where now P is the pressure in torr and M is the molecular weight of the gas (g/mole).

Let us now consider the adsorption of oxygen. In theis case one expects Eq. 12 to apply since ΔH_a (= 110 Kcal/mole) is quite large. Taking the reasonable values s = 0.3 (11), T_g = 150°K (about one-half of the specimen temperature) and N = 2 x 10^{15} molecules/cm^2, the exposure (Pt) which gives a monolayer of oxygen on the copper is 1.8 x 10^{-5} torr-second. This value compares very well with the exposure in Fig. 24 where the cohesion coefficient is beginning to decrease rapidly.

It is also of interest to compare the present results with the adsorption of oxygen on copper as determined by LEED studies. The Leed results by Simmons et (15) for the adsorption of oxygen on the (110), (100) and (111) faces of copper single crystals are summarized in Table VI,

Table VI (15)
Summary of Structures on Copper Observed by LEED

Surface Orientation	Observed Structures	Oxygen Exposures	Remarks
(110)	One-dimentional structure ordered only in the [001] direction	3×10^{-8} Torr min	
	(2×1)	2×10^{-5} Torr min	
	Mixed (2×1) and $c(6 \times 2)$	2×10^{-4} Torr min	
	$c(6 \times 2)$	6×10^{-1} Torr min	500 °C
	thermal faceting	6×10^{-4} Torr	500-700 °C
(100)	"four-spot structure"	1×10^{-6} Torr min	Not always observed with initial oxygen exposure of clean surface
	$p(1 \times 1)$	5×10^{-5} Torr min	Unstable to mild temperature treatment; low temperature annealing resulted in the (2×1)
	(2×1)	1×10^{-4} Torr min	Two orientations rotated by 90° are required to explain diffraction pattern
	thermal faceting	5×10^{-4} Torr	400-700 °C
(111)	monolayer O^{2-}	4×10^{-5} Torr min	Measured diameter of O^{2-} of 3.11Å compares favorably with crystallographic value of 2.80Å
	coincide lattice	1.5×10^{-3} Torr min	Six orientations of this unit mesh are possible; only two were observed

which was taken from their paper. These studies indicate that for the (110) and (100) faces initial adsorption of oxygen (up to exposures of about 10^{-5} torr-second) occurs by random adsorption of oxygen atoms. Beyond about 10^{-5} torr-second a new structure starts to form which becomes fully developed at about 10^{-3} torr-second. This new structure is a (2 x 1) structure and appears to consist of both copper and oxygen atoms. Further increase of exposure to 10^{-2} torr-second merely serves to intensify this "reconstructed" surface structure. For the (111) face, the initial stage appears to be the adsorption of O^{-2} ions, which at an exposure of 10^{-2} torr-second form a coincidence lattice with the copper atoms of the surface.

Comparing the effect of exposure to O_2 on the cohesion of copper presented in Fig. 24 with the LEED results and the above calculation for the exposure required to form a monolayer, one is led to the following conclusions: The cohesion coefficient decreases slightly by the adsorption of oxygen atoms (or ions) up to the formation of a monolayer, after which a much more rapid decrease occurs. Associated with this rapid decrease is the formation of the new (2 x 1) structure on the (110) and (100) faces and the coincidence structure on the (111) face. The cohesion coefficient reaches its minimum value once these structures are fully developed ($\sim 10^{-2}$ torr-second).

Let us now consider the adsorption of CO and CO_2 on copper. In view of the lower energy for the adsorption of these gases, one expects that Eq. 11 will apply. The exposures (Pt) to these gases were obtained by increasing the pressure, the time being constant at 600 seconds. The reduced cohesion resulting from the exposure to these gases can therefore be considered to be due to the increase in amount of adsorbed gas with increased pressure. If this is so, one can then obtain an estimate of the energy of adsorption of CO and CO_2 from the cohesion results using Eq. 11. Rearranging Eq. 11 gives

$$\Delta H_a = RT_s \ln \left[\frac{Ne\ (MT_g)^{1/2}}{3.5 \times 10^{22}\ sP\tau_o} \right] \qquad (13)$$

For CO, reasonable values for s and τ_o are: $s = 0.3$, $\tau_o = 2 \times 10^{-13}$ sec. (14). Moreover, it is assumed that a monolayer of gas is absorbed when the cohesion coefficient has decreased to the value 0.86 obtained when there exists a monolayer of oxygen (calculated above). This value of the cohesion coefficient occurs for CO at a pressure of 1.6×10^{-6} torr. Substituting these values of s, τ_o and P into Eq. 13 gives ΔH_a for CO on copper equal to 18.5 Kcal/mole, which is within the range of measured values (Table III). A similar value is obtained from the cohesion results for the adsorption energy of CO_2 onto copper.

5. CONCLUSIONS

The following conclusions can be drawn from the present investigation:

1. The technique of cold welding specimens previously fractured in an ultrahigh vacuum yields cohesion results which are in good accord with those obtained using more elaborate techniques of surface preparation and testing, and hence represents a convenient technique for studying surface phenomena.

2. The cohesion coefficient for "clean" surfaces of all FCC metals investigated by all the various techniques reported in the literature (including the results presented here for the fracture technique) ranges from 0.62 to 1.15, the lower values being obtained for the lower stresses and for specimens in a severely cold worked state.

3. It is proposed that the reason for the essentially constant cohesion coefficient for the ductile FCC metals is that the area of contact for a given load is inversely proportional to the flow (or fracture) stress of the material and the bond strength is directly proportional to this flow (or fracture) stress.

4. In the present investigation using the fracture technique, the effect of compressive load (or stress) on the cohesion coefficient for all the FCC metals considered could be normalized through the original fracture strength of the virgin specimen. These results give support to the conclusion immediately above.

5. The effect of various gases on the cohesion of Cu was found to be related to the degree of adsorption on the surface. Weakly physiadsorbed N_2 had no effect on the cohesion up to pressures of 760 torr at room temperature. Strongly chemiadsorbed O_2 significantly reduced the cohesion coefficient after the adsorption of a monolayer. Strongly physiadsorbed (or weakly chemiadsorbed) CO and CO_2 significantly reduced the cohesion coefficient at pressures above about 10^{-6} torr.

6. Comparison of LEED results for the adsorption of oxygen onto the faces of single crystals of Cu with the present cohesion results indicates that the most rapid decrease in cohesion coefficient coincides with the formation of the "reconstructed" (2 x 1) structure on the (110) and (100) faces and the coincidence lattice of oxygen ions on the (111) faces.

7. An adsorption energy of 18.5 Kcal/mole for CO and CO_2 on Cu was calculated from the cohesion results using adsorption theory. This is within the range of experimental values reported for the adsorption of these gases on Cu.

8. The cohesion coefficient for 70-30 brass was only about one half that for pure copper. A lower cohesion coefficient resulted following heat treatments of 1 hour at 300°C and 1 hour at 600°C of the cold weld in tough pitch copper. The reasons for these reductions in cohesion coefficient are not clear.

6. REPORTS AND PUBLICATIONS

I. Technical Reports

1. H. Conrad and L. Rice, "Colding Welding of Copper Under Ultrahigh Vacuum" FIRL Report SA-B2368-4. Oct. 1, 1966 to March 31, 1967.

II. Publications in Technical Journals

1. H. Conrad and L. Rice, "Cold Welding of Copper Under Ultrahigh Vacuum", *Adhesion or Cold Welding of Materials in Space Environments*, ASTM STP 431, p. 208-233 (1967).

7. REFERENCES

1. R. W. Roberts and L. E. St. Pierre, *Science, 147,* 1529 (1965).

2. R. M. Evans and R. E. Monroe, "Surface Welding in the Space Environment", *DMIC Memo 214,* June 9, 1966.

3. J. L. Ham, *ASLE Trans. 6,* 20 (1963).

4. H. Schwartzbart and W. Brown, *Trans. ASM, 46,* 998, (1954).

5. N. Brown and K. F. Lukens, *Acta Met, 9,* 106, (1961).

6. H. Conrad, *High Strength Materials,* Wiley, p. 436, (1965).

7. H. Conrad, "Work Hardening Model for the Effect of Grain Size on the Flow Stress of Metals" to be publ. 2nd General Assembly of CENIM, Madrid, Spain (10-13 June, 1969).

8. L. G. Kellog, *Adhesion or Cold Welding of Materials in Space Environments*, ASTM STP 431, p. 181 (1967).

9. W. P. Gilbreath, ibid p. 128.

10. H. Conrad and L. Rice, ibid. p. 208.

11. D. O. Hayward and B. M. W. Trapnell, *Chemisorption,* Butterworths, London (1964).

12. H. Shen, S. E. Podlasek and I. R. Kramer, Trans. AIME *233* 1933 (1965).

13. I. R. Kramer and S. Podlasheck, Acta Met. *11* 70 (1963).

14. W. P. Gilbreath, "The Influence of Gaseous Environment on the Self-Adhesion of Metals," NASA TN D-4868 (Oct. 1968).

15. G. W. Simmons, D. F. Mitchell and K. L. Lawless, Surface Science *8* 130 (1967).

UNCLASSIFIED
Security Classification

DOCUMENT CONTROL DATA - R & D

Security classification of title, body of abstract and indexing annotation must be entered when the overall report is classified)

1. ORIGINATING ACTIVITY (Corporate author) The Franklin Institute Research Laboratories Philadelphia, Pa. 19103 H. Conrad and L. Rice	2a. REPORT SECURITY CLASSIFICATION None 2b. GROUP ---

3. REPORT TITLE

A BASIC STUDY OF COLD WELDING IN ULTRAHIGH VACUUM

4. DESCRIPTIVE NOTES (Type of report and inclusive dates)

Final Technical Report, May 30, 1969

5. AUTHOR(S) (First name, middle initial, last name)

Hans Conrad, L. Rice

6. REPORT DATE	7a. TOTAL NO. OF PAGES	7b. NO. OF REFS
May 30, 1969	83	15

8a. CONTRACT OR GRANT NO	9a. ORIGINATOR'S REPORT NUMBER(S)
Nonr 4825(00), NR 031-078 b. PROJECT NO c. d.	F-B2368 9b. OTHER REPORT NO(S) (Any other numbers that may be assigned this report)

10. DISTRIBUTION STATEMENT

Distribution of this document is unlimited.

11. SUPPLEMENTARY NOTES	12. SPONSORING MILITARY ACTIVITY
	Office of Naval Research Department of the Navy Washington, D.C. 20360

13. ABSTRACT

The cohesion of the FCC metals Ag, Al, Cu, and Ni, under ultrahigh vacuum (10^{-11} to 10^{-9} torr) was investigated by cold welding specimens previously fractured in the vacuum. The cohesion strength of the weld increased with compression load for all metals; all data fell on one curve of slight positive curvature when the cohesion load (stress) and the compression load (stress) were divided by the initial fracture load (stress) of the virgin specimen. The effect of compression load on the cohesion coefficient α, for all metals could be described by $\alpha = 0.75 + 0.15\ L_C/L_{F_o}$, where L_C is the compression load and L_{F_o} is the initial fracture load. Ultrasonic measurements and microscopic examination of ^{o}Cu specimens indicated that the contact area was proportional to the ratio L_C/L_{F_o} and that excellent matching of the fractured surfaces was possible with the apparatus used. The cohesion results are explained on the basis that the rupture of the weld occurs at a constant value of the "true" fracture stress.

Heat treatment reduced the strength of copper welds and alloying (70-30 Brass) lowered the cohesion coefficient compared to unalloyed Cu. Prolonged exposure of copper fracture surfaces to the gases O_2, CO, CO_2 and air caused an appreciable reduction in the cohesion coefficient, whereas no effect was observed for N_2. This is in good agreement with predictions based on absorption theory and observations reported for LEED studies.

DD FORM 1 NOV 65 1473

UNCLASSIFIED
Security Classification

14. KEY WORDS	LINK A		LINK B		LINK C	
	ROLE	WT	ROLE	WT	ROLE	WT
Cold Welding Cohesion Fracture						